

12-14-2001

Measuring the Effects of Soil Parameters on Bidirectional Reflectance Distribution Function

Pushkar Shrikant Pradhan

Follow this and additional works at: <https://scholarsjunction.msstate.edu/td>

Recommended Citation

Pradhan, Pushkar Shrikant, "Measuring the Effects of Soil Parameters on Bidirectional Reflectance Distribution Function" (2001). *Theses and Dissertations*. 3036.
<https://scholarsjunction.msstate.edu/td/3036>

This Graduate Thesis - Open Access is brought to you for free and open access by the Theses and Dissertations at Scholars Junction. It has been accepted for inclusion in Theses and Dissertations by an authorized administrator of Scholars Junction. For more information, please contact scholcomm@msstate.libanswers.com.

MEASURING THE EFFECTS OF SOIL PARAMETERS ON BIDIRECTIONAL
REFLECTANCE DISTRIBUTION FUNCTION

By

Pushkar Shrikant Pradhan

A Thesis
Submitted to the Faculty of
Mississippi State University
in Partial Fulfillment of the Requirements
for the Degree of Master of Science
in Electrical Engineering
in the Department of Electrical and Computer Engineering

Mississippi State, Mississippi

December 2001

MEASURING THE EFFECTS OF SOIL PARAMETERS ON BIDIRECTIONAL
REFLECTANCE DISTRIBUTION FUNCTION

By

Pushkar Shrikant Pradhan

Approved:

Roger L. King
Professor of Electrical and
Computer Engineering
(Director of Thesis)

A. Wayne Bennett
Dean of the College of
Engineering

Michael Cox
Associate Professor of Soil
Science
(Committee Member)

Nicolas Younan
Professor of Electrical and
Computer Engineering
(Graduate Coordinator and
Committee Member)

Name: Pushkar Shrikant Pradhan

Date of Degree: December 14, 2001

Institution: Mississippi State University

Major Field: Electrical Engineering

Major Professor: Dr. Roger King

Title of Study: MEASURING THE EFFECTS OF SOIL PARAMETERS ON
BIDIRECTIONAL REFLECTANCE DISTRIBUTION FUNCTION

Pages in Study: 99

Candidate for the Degree of Master of Science

Remote sensing data acquisition often requires a revisit to the same target. Therefore, it is not always possible to have the same illumination and viewing conditions. Bidirectional Reflectance Distribution Function (BRDF) is an attempt to predict the reflectance of an object for any given viewing and illumination geometry by explaining the interaction of the incident energy with the target object, the medium lying between the source and the target, and the interaction of the reflected energy with the medium between the target and the sensor. In this study various factors affecting BRDF were explored. Various factors contribute to this characteristic of the surface to reflect unequally in different directions like its structure, shape, degree of absorption and transmittance. Bidirectional Reflectance Factor, Anisotropic Factor, and Anisotropic Index were used in the research. Radiances were recorded using the Sandmeier Field Goniometer of target areas at the agricultural farms of Mississippi State University.

DEDICATION

I would like to dedicate this research to my parents, Shrikant and Alka Pradhan,
and my brother Advait.

ACKNOWLEDGEMENTS

I would like to express my deepest gratitude to my advisor Dr. Roger L. King, who guided me through every step of writing this project. I particularly thank Dr. King for his support and his valuable time in reviewing the thesis draft and discussing various important issues encountered during the development and writing of this project. I would also like to take this opportunity to thank the members of my committee, Dr. Michael Cox and Dr. Nicolas Younan for their help and guidance.

TABLE OF CONTENTS

	Page
DEDICATION	ii
ACKNOWLEDGEMENTS	iii
LIST OF TABLES	vii
LIST OF FIGURES	viii
CHAPTER	
I. INTRODUCTION TO THE BRDF PHENOMENON	1
II. BIDIRECTIONAL REFLECTANCE DISTRIBUTION FUNCTION	4
Image Analysis.....	5
Applications To Precision Agriculture	6
Bidirectional Reflectance Distribution Function	7
Lambert’s cosine law and Lambertian surface	7
Scattering	9
Factors affecting BRDF	11
Surface Orientation	11
Particle Density and Size	11
Definition of terms in BRDF	13
Solar Principal Plane.....	13
Orthogonal Principal Plane	13
Bidirectional Reflectance Factor.....	14
Anisotropy Factor	15
Anisotropy Index	16
Mean Anisotropic Index	18
Hemispherical Reflectance	18
Calculation of Hemispherical Reflectance.....	19
III. EXPERIMENTAL DETAILS AND THE GONIOMETER	21
Introduction and motivation for the SFG	21
Technical specifications of the SFG	21

CHAPTER	Page
Sensor Details	22
Operation.....	23
Data Log.....	25
Space/Time Tradeoff	26
Site Location and Description.....	26
Site Location	26
Site Description.....	28
Ridged	28
Disked and Fallow	29
Zoysia Grass.....	30
Experimental Details.....	31
IV. RESULTS	33
Causes of anisotropy.....	33
Shadowing effects.....	33
Soil Roughness.....	45
Effect on Reflectance.....	46
Effect on Anisotropy.....	47
Soil Moisture.....	50
Effect on Reflectance.....	50
Effect on Anisotropy.....	52
Effect of digging the hole	56
Zoysia Grass.....	57
Comparison of Anisotropy of different sites	61
V. CONCLUSIONS.....	63
Soil surface structure.....	63
Ground terrain.....	64
Soil moisture	64
Recommendations and future work	64
Errors due to Non-Lambertian and lossy panel	64
Effect of Diffuse Irradiance	65
Anisotropy as a function of the Surface Roughness	66
Multiple Data Sets.....	69
Suggestions to Improve the Data Acquisition Time of the SFG	70
REFERENCES	71
APPENDIX	
A. Table of symbols.....	73

APPENDIX

Page

B. IDL code75

LIST OF TABLES

TABLE		Page
3.1	Details of each test site	27
3.2	Sun position and timings for each experiment.....	32
4.1	Mean ANIX values	62
5.1	Details of the MMR experiment	67

LIST OF FIGURES

FIGURE		Page
1.1	The remote sensing phenomenon.....	2
2.1	Lambertian surfaces	8
2.2	The coordinate system	10
2.3	Specular reflectance	12
2.4	Diffuse reflectance	12
2.5	The solar and orthogonal principal planes	14
2.6	Anisotropy in different azimuth planes in the fallow soil.....	17
3.1	The Sandmeier Field Goniometer.....	22
3.2	Sampling scheme for the goniometer	24
3.3	Ridged Soil.....	28
3.4	Disked Soil.....	28
3.5	Fallow Soil	28
3.6	Zoysia Grass.....	28
3.7	Position of the different spots in the ridged soil	29
4.1	Ridged soil	34
4.2	Reflectance in the ridged soil (valley spot).....	36
4.3	Reflectance in the ridged soil (shaded spot)	37
4.4	Reflectance in the ridged soil (peak spot).....	38
4.5	Reflectance in the ridged soil (sunny spot).....	38
4.6	Anisotropy in the ridged soil (valley spot)	40
4.7	Anisotropy in the ridged soil (shaded spot)	41
4.8	Anisotropy in the ridged soil (peak spot).....	42

FIGURE	Page
4.9	Anisotropy in the ridged soil (sunny spot).....43
4.10	Hemispherical reflectance at different spots (ridged soil)44
4.11	Anisotropy in the principal plane for the ridged soil spots.....45
4.12	Hemispherical reflectance in the three soils46
4.13	Anisotropy indices (SPP) of the three soils47
4.14	Anisotropy in the fallow soil (dry condition)48
4.15	Anisotropy in the disked soil49
4.16	Albedo under different conditions51
4.17	ANIX for different conditions in the fallow soil52
4.18	Anisotropy in the fallow soil (dry).....53
4.19	Anisotropy in the fallow soil (hole).....54
4.20	Anisotropy in the fallow soil (wet).....55
4.21	Anisotropy in the fallow soil (flooded).....56
4.22	Anisotropy in the zoysia grass (9:24 A.M).....57
4.23	Anisotropy in the zoysia grass (9:47 A.M).....58
4.24	Anisotropy in the zoysia grass (3:03 P.M).....59
4.25	Albedo in the zoysia grass60
5.1	Anisotropy (in the SPP) of the three soils.....68

CHAPTER I

INTRODUCTION TO THE BRDF PHENOMENON

Remote sensing is the process of measuring some property of a target from a distance, without coming into direct contact with it. There are three components to remote sensing: 1) the source, 2) the target and 3) the sensor. The energy emitted by the source strikes the target. Upon interaction with the target some properties of the energy are changed (e.g. its amplitude, phase etc.). The sensor looking towards the target records a part of this energy reflected from the target. This reflected energy can be used to make inferences about the target like its temperature, color, or size. Figure 1-1 illustrates the remote sensing process. The source of energy in remote sensing is active or passive electromagnetic energy. Another example is acoustic energy, used in underwater remote sensing (SONAR).

Electromagnetic energy striking an object is reflected, absorbed and transmitted as seen in Figure 1-1. The symbols used in this illustration are explained in Appendix A. In remote sensing, emphasis is placed on the reflected portion of the incident energy since it is easy to measure compared to the absorbed and transmitted portions.

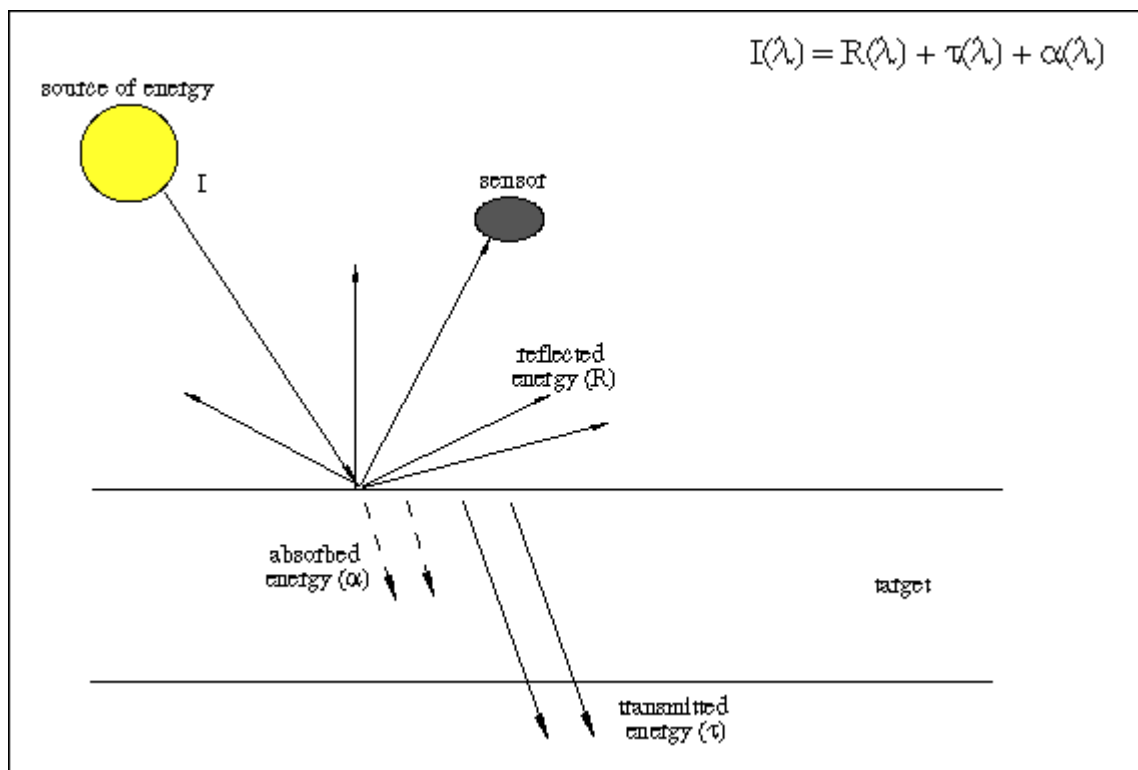


Figure 1-1: The remote sensing phenomenon

With the increasing availability and economic feasibility of satellites, many of the remote sensing projects are carried out from space-borne platforms. Satellite-based remote sensing is cost-effective, fast and provides repetitive coverage. However, there are numerous technical difficulties associated in preserving the information in the data ranging from the hardware problems of the sensor, hazy atmosphere, to non-Lambertian targets. These factors must be analyzed and accounted for prior to data interpretation.

In this work we studied various factors affecting soil Bidirectional Reflectance Distribution Function (BRDF) using a ground instrument called the Sandmeier Field Goniometer (SFG), which employs a hyperspectral sensor. Chapter two explains the significance of BRDF in remote sensing and lists some principal factors responsible for the BRDF phenomenon. Definitions of various terms used to study BRDF, are also given.

The working of the Sandmeier Field Goniometer and a detailed description of the data sets are presented in chapter three. The findings are reported in chapter four along with theories to explain them. The limitations of this study and guidelines for future work are discussed in chapter five. Suggestions to improve the data acquisition of the SFG are also given.

CHAPTER II

BIDIRECTIONAL REFLECTANCE DISTRIBUTION FUNCTION

Remote sensing of the earth takes place from air-borne as well as space-borne platforms. The data acquisition methods have advanced from simple black and white photographs to multispectral digital imagery to hyperspectral data. There are numerous applications and advantages of the remotely sensed data. A few of them are mentioned here: 1) Vast regions of the earth can be mapped in a few days, 2) Weather forecasts and 3) Environmental monitoring.

Artificial satellites orbiting the earth are continuously capturing the images of the earth falling within their footprint. The onboard sensor samples the incoming radiance at frequent intervals in the spectrum and stores it in the form of 8 or 16-bit digital numbers (DNs). There is a wealth of information stored in these DNs about the surface mapped. However, the data acquisition process is never perfect, thus the quality of the recorded images is degraded. The degradations are due to geometric distortion, radiometric distortion and noise. Radiometric distortion is closely associated with BRDF.

Image Analysis

The DNs recorded by the same sensor for the same scene can be quite different on a revisit. The following factors are responsible for this: The illumination conditions at the same place at the same time of the day are different on different dates because of the elliptical path of the sun, resulting in low irradiance in winter when it is farthest away and high irradiance in summer when it is closest to the earth.

- 1) Suspended particles like smoke, haze, and water vapor in the atmosphere cause scattering. Thus the irradiation at the target is not just due to the direct rays of the sun, but also due to diffuse radiation caused by suspended matter. Even at the sensor the recorded radiance is a sum of the radiation reflected back by the target and also the diffuse radiation. The concentration of suspended particles in the atmosphere changes with the time and day, which makes it more difficult to account for the diffuse radiation.
- 2) Sensors are capable of viewing the same spot from more than one angle (e.g. the SPOT sensors have this capability). This trend is becoming increasingly popular with the new satellites that are being launched. Thus, a given location on earth can be monitored for a longer time than possible with a fixed look sensor. Though this is an advantage, reflectance of the same spot observed from different viewing directions is generally different.

Some of the applications of satellite imagery are classification and land change detection of a large area. A classification project involves assigning pixels of the digital image to various categories like deserts, forests, agricultural land and water bodies based

on some 'a priori' knowledge. In a change detection project imagery of the same region taken from two or more dates is compared to find out the environmental changes in the region. This requires images taken from different dates to do the classification. Image processing software used for such tasks use the reflectance values (recorded DN's) of individual pixels to assign them to different categories like land, water, forests, pastures etc. Classification is often based upon the relative DN of the pixels. For example, pines and hardwoods can be differentiated on the basis of their different reflectance values. However, it would be possible that both have identical reflectance for two different illumination conditions. This leads to confusion and error in classification. Thus, there is need for some sort of normalization. A common practice is to normalize the reflectance values of the pixels to a common illumination and view angle (usually the nadir).

Applications to Precision Agriculture

In order to maximize profits, farmers are looking towards precision agriculture to increase their yield while minimizing production costs incurred on items like pesticides, seeds, and fertilizers. This requires frequent imaging of the site to determine nutrient prescriptions or stress sources [7] at a regular interval throughout the growing season. However, there will be discrepancies in the imagery due to the changing target (e.g., change in biomass, effect of rainfall on the soil moisture), varying illumination and viewing geometry. It is impossible to control weather or the sun's position.

Decisions regarding soil management, irrigation and application of pesticides are made based upon the analysis of this imagery. If the BRDF factors are neglected they could lead to erroneous conclusions and faulty crop management decisions.

Bidirectional Reflectance Distribution Function

Before dealing with Bidirectional Reflectance Distribution Function it is necessary to understand the following topics:

- 1) Lambert's cosine law and Lambertian surfaces
- 2) The scattering phenomenon

Lambert's cosine law and Lambertian surface

Lambertian Surface: The radiance (brightness) of a lambertian surface remains constant with the viewing direction. The sun is an excellent example of a Lambertian surface. MgO , $BaSO_4$, snow and certain paints are also examples of Lambertian surfaces [9].

Let there be a radiator of area dS radiating power with intensity I_n (units: $watts \cdot sr^{-1}$) in the direction of its normal as shown in figure 2-1. The radiance L_n (units: $watts \cdot sr^{-1} \cdot m^{-2}$) in the direction of the normal is given by equation 2.1.

$$L_n = \frac{I_n}{dS} \quad (2.1)$$

Lambert's cosine law governs the radiant intensity of a lambertian surface in any given direction. This law states that the radiant intensity I_θ at a given point is equal to the product of the radiant intensity in the normal direction I_n and the cosine of the angle θ between a line joining the point to the surface and the normal to the surface. Mathematically this relationship is given in equation 2.2 [6]. Thus the radiant intensity of a Lambertian surface in a given direction is falling with the cosine of the angle between

the normal and the line joining this point to the surface. However, the perceived area of the radiator at this point is also decreasing with the cosine of this angle. The perceived area at an angle θ is given by equation 2.3. The radiance in any direction L_θ is given by equation 2.4. Substituting equations 2.2 and 2.3 into 2.4 we see that the radiance in any given direction is equal to the radiance in the normal direction. Equation 2.5 gives the mathematical proof for a Lambertian surface.

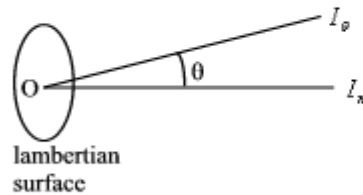


Figure 2-1: Lambertian surfaces

$$I_\theta = I_n \cos \theta \quad (2.2)$$

$$dS_\theta = dS \cos \theta \quad (2.3)$$

$$L_\theta = \frac{I_\theta}{dS_\theta} \quad (2.4)$$

$$L_\theta = L_n \quad (2.5)$$

Scattering

The phenomenon of scattering is responsible for some of the BRDF effects observed. This report will first explain how it occurs and then describe some of the factors that control the way in which scattering occurs.

Definition: When incident energy strikes a particle, some part of it is absorbed (by the particle), transmitted (through the particle) and the rest is reradiated in different directions. The sum of the reradiated energy in all the directions is known as the scattered energy.

The intensity of scattering depends on the ratio of the particle size to the wavelength of the incident wave. Scattering can be classified into two types:

- 1) Rayleigh scattering: It occurs when the particle size is smaller than the wavelength of the incident energy. Atmospheric molecules are examples of particles that cause this type of scattering.
- 2) Mie scattering: It occurs when the particle size is greater than the wavelength. Aerosols (smoke, smog and haze) and hydrometeors (mist, rain, snow, hail, fog and clouds) are examples of Mie scatterers.

Generally the scattered ray is scattered repeatedly by other particles in the vicinity. This phenomenon is known as multiple scattering. Thus there are two components of the scattered light [3] - 1) singly scattered and 2) multiply scattered.

Figure 2-2 [6] explains the coordinate system used to explain the definitions of BRDF and other BRDF related indices given below. Appendix A is a table of symbols used to explain the various definitions.

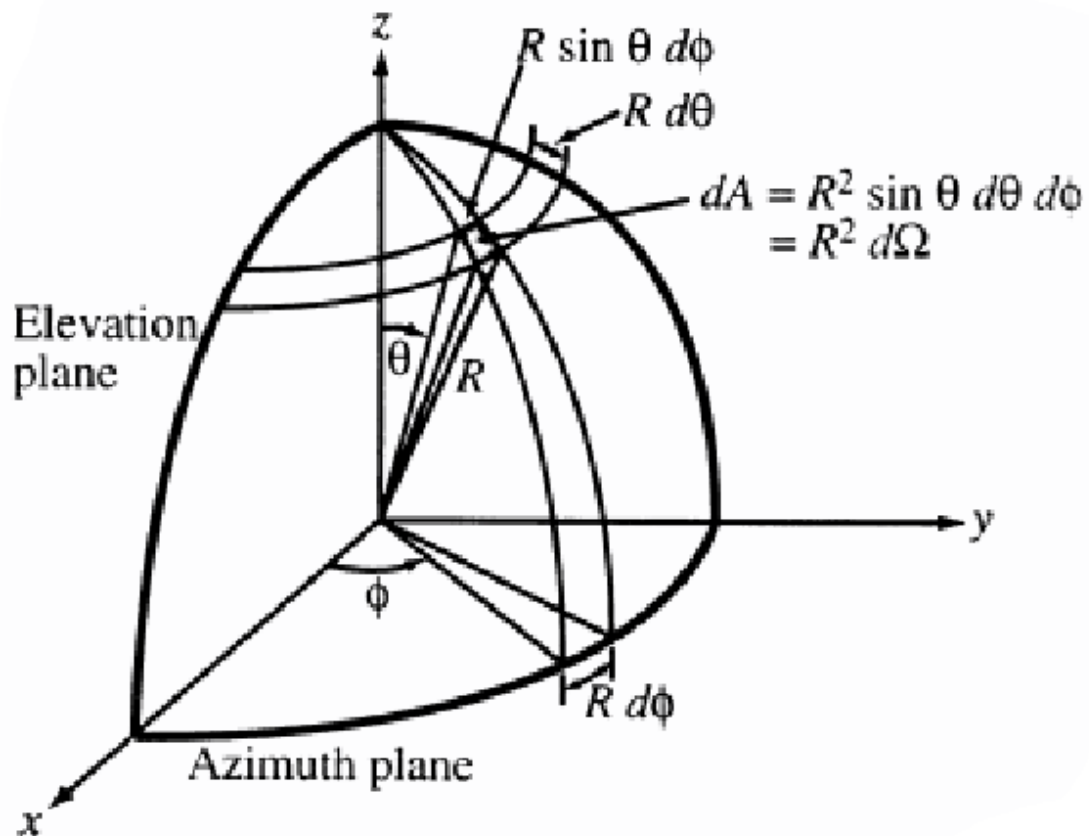


Figure 2-2: The coordinate system

Definition: BRDF is the ratio of the radiance dL_r (unit: $\text{W}\cdot\text{m}^{-2}\cdot\text{sr}^{-1}\cdot\text{nm}^{-1}$) reflected from the surface of the target into the direction (θ_v, ϕ_v) to the incident irradiance I (unit: $\text{W}\cdot\text{m}^{-2}\cdot\text{nm}^{-1}$) illuminating the surface from a direction (θ_i, ϕ_i) [8]. Thus the unit of BRDF is $[\text{sr}^{-1}]$. This can be written mathematically as follows:

$$BRDF(\theta_v, \phi_v, \theta_i, \phi_i) = \frac{dL_r(\theta_v, \phi_v; \lambda)}{I(\theta_i, \phi_i; \lambda)}, \quad (2.6)$$

The irradiance intensity at the target varies with the source position - $\langle \theta_i, \phi_i \rangle$ (high in the noon and low in the mornings and evenings) and the wavelength. The measured radiance, also changes with the sensor position - $\langle \theta_v, \phi_v \rangle$, thus BRDF is a function of the source position, sensor position and the wavelength.

Factors affecting BRDF

The amount of radiance reflected from the target in a particular view direction for a given illumination is a function of the geometrical and optical properties of the surface. Surface orientation with respect to the source, particle density, particle size, absorption and transmittance of the surface are some of the principal factors affecting BRDF. Each of them will be explored in detail.

Surface Orientation

The orientation of the surface with respect to the source directly affects the amount of shadowing and its distribution. A sensor looking at a target on the western slope of a mountain in the morning would record low reflectance while high reflectance would be measured in the evening at the same spot assuming the same atmospheric cloudiness.

Particle Density and Size

The reflected energy reaching the detector consists of the incident ray reflected only once from the surface to the sensor without coming into contact with any other

particle and other rays which were reflected multiple times from other particles into the field-of-view of the sensor.

The interspacing and size of the particles, which make up the structure, determine whether the singly scattered or the multiply scattered term dominates. The orientation of individual particles determines the path taken by the incident and reflected rays. When the particles are spaced far apart relative to each other the singly scattered component dominates, causing a specular reflectance (figure 2-3). An increase in the particle density increases the multiply scattered component. This leads to diffuse reflectance. This is illustrated in figure 2-4.

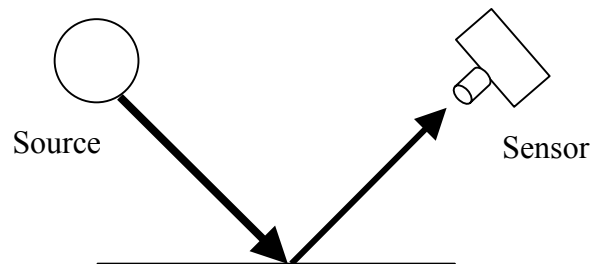


Figure 2-3: Specular reflectance

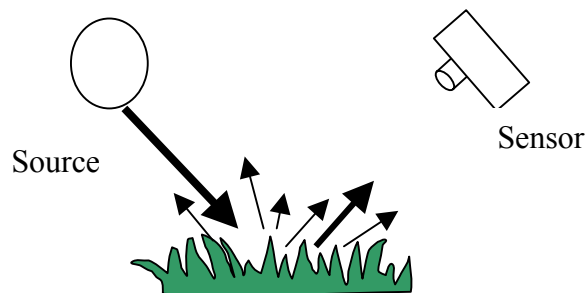


Figure 2-4: Diffuse reflectance

When incident energy strikes a target it can either be: 1) reflected, 2) transmitted and/or 3) absorbed. Thus as the amount of energy absorbed by the target increases, the reflected portion decreases due to the law of conservation of energy. This results in lower values being recorded at the sensor. Similar results are observed when the transmittance of the object is high.

A qualitative analysis of the BRDF of a target is not sufficient. Often it is necessary to make a quantitative estimate of the deviation of the target from the ideal Lambertian behavior. Researchers have come up with various indices in an attempt to quantify the non-Lambertian properties of a target. A few of them used in this study are - Bidirectional Reflectance Factor (BRF), Anisotropy Factor (ANIF), Anisotropy Index (ANIX) and Hemispherical Reflectance (ρ).

Definition of terms in BRDF

Solar Principal Plane

Definition: The plane containing the source of energy (e.g. the sun), the target and the sensor is called the solar principal plane (SPP).

Orthogonal Principal Plane

Definition: The plane perpendicular to the solar principal plane is called the orthogonal principal plane (OPP).

Figure 2-5 illustrates the concept of solar and orthogonal principal plane. The line with the short dashes represents the SPP while the line with the long dashes represents the OPP.

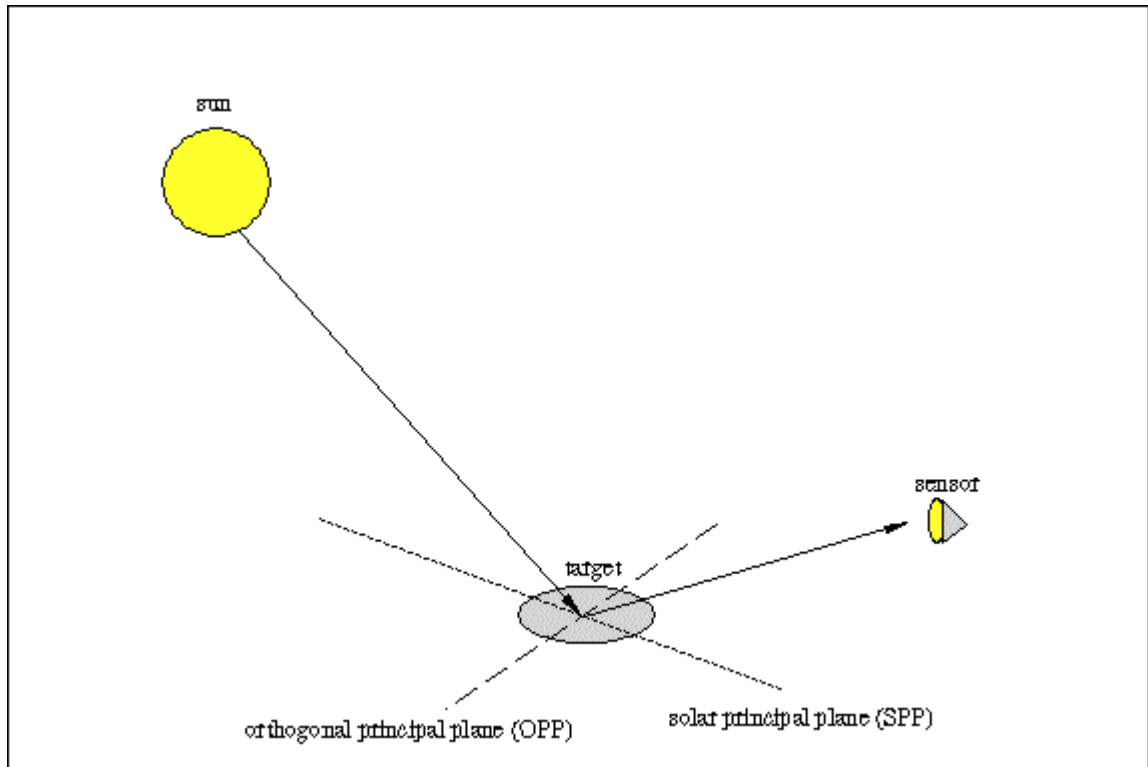


Figure 2-5: The solar and orthogonal principal planes

Bidirectional Reflectance Factor

Definition: The ratio of the radiance dL_r reflected from the target in the direction $\langle \theta_v, \phi_v \rangle$ to the radiance dL_{ref} reflected from a loss-less Lambertian reflectance-reference panel in the same direction measured under identical illumination conditions is known as the Bidirectional Reflectance Factor [13].

The measured radiance depends on the incident illumination $I(\theta_i, \phi_i, \lambda)$, the direction of the sensor $\langle \theta_v, \phi_v \rangle$ with respect to the surface and the wavelength (λ) thus the BRF is a function of all these quantities. Mathematically this can be written as follows:

$$BRF(\theta_v, \phi_v; \theta_i, \phi_i; \lambda) = \frac{dL_r(\theta_v, \phi_v; \theta_i, \phi_i; \lambda)}{dL_{ref}(\theta_v, \phi_v; \theta_i, \phi_i; \lambda)}, \quad (2.7)$$

An ideal loss-less Lambertian panel reflects all the energy, incident upon it (dL_{ref}) in all directions equally. Since BRF is a ratio of two similar quantities (radiance) it is unit-less.

If the exact definition of BRF is followed then it implies that the radiances must be measured in infinitesimally small angles. Current sensors have a fixed field-of-view and thus the BRF values measured are a result of the contribution of radiances within a small solid angle around the target point and thus, they must be referred to as 'biconical reflectance factors'. However, it is not possible to construct sensors with an infinitesimal field-of-view. However, the quantities measured with these sensors are accepted as the bidirectional reflectance factors. Research has demonstrated that they characterize the BRDF phenomenon.

Anisotropy Factor (ANIF)

An ideal Lambertian (isotropic) surface radiates equally in all directions, thus the observed reflectance (BRF) in any direction will be identical. Unfortunately most surfaces in nature are non-Lambertian (anisotropic), i.e. they do not radiate equally in all directions. Different surfaces exhibit different degrees of anisotropy. For example, concrete, which exhibits diffuse reflectance, has a lower anisotropy compared to water, which has a higher anisotropy due to specular reflectance (a sharp glint is observed when looking at water bodies from certain directions, [7]). Thus to measure the degree of

anisotropy of a surface we need a reference quantity, generally the nadir reflectance is used for this purpose.

Definition: The anisotropy factor of a surface in a particular view direction $\langle \theta_v, \phi_v \rangle$ is defined as the ratio of the reflectance in that direction to the nadir reflectance $\langle \theta_v = 0^\circ, \phi_v = 0^\circ \rangle$ [13]. Since ANIF is a ratio of two reflectance factors it is also a unit-less quantity. Mathematically it can be stated as follows:

$$ANIF(\theta_v, \phi_v; \theta_i, \phi_i; \lambda) = \frac{BRF(\theta_v, \phi_v; \theta_i, \phi_i; \lambda)}{BRF(0^\circ, 0^\circ; \theta_i, \phi_i; \lambda)}, \quad (2.8)$$

The ANIF values for an ideal Lambertian surface would be unity in all view directions.

Anisotropic Index

Definition: The ratio of the maximum and the minimum reflectance factors observed in a given azimuth plane for a given spectral band is known as the Anisotropy Index [12]. Since this quantity is also a ratio of two BRFs it is a unit-less quantity. The mathematical definition is as follows:

$$ANIX(\theta_v; \theta_i, \phi_i; \lambda) = \frac{BRF_{\max}(\theta_1, \phi_v; \theta_i, \phi_i; \lambda)}{BRF_{\min}(\theta_2, \phi_v; \theta_i, \phi_i; \lambda)}, \quad (2.9)$$

In this equation θ_1 and θ_2 are the zenith angles in the azimuth plane - ϕ_v where the maximum and the minimum reflectance factors are observed.

It describes the variation of the reflectance in any given azimuth plane. To understand the anisotropy of a target, generally the ANIX values in the solar principal

plane (SPP) are investigated, Sandmeier [13] suggests that the reflectance values exhibit maximum contrast in the SPP; the contrast decreases as the sensor moves to the orthogonal principal plane (OPP). To verify this fact we plotted the ANIX values in all the azimuth planes for all the data sets we collected. The results are in agreement with Sandmeier's statement. Thus it was deemed best to use the ANIX terms in the SPP for comparison between two or more data sets. Figure 2-6 shows the ANIX values in all the azimuth planes for measurements collected on fallow soil. The fallow soil has a smooth and flat surface. The surface layer is very dark grayish-brown silty clay loam. For conciseness the plots corresponding to the other data sets are not shown.

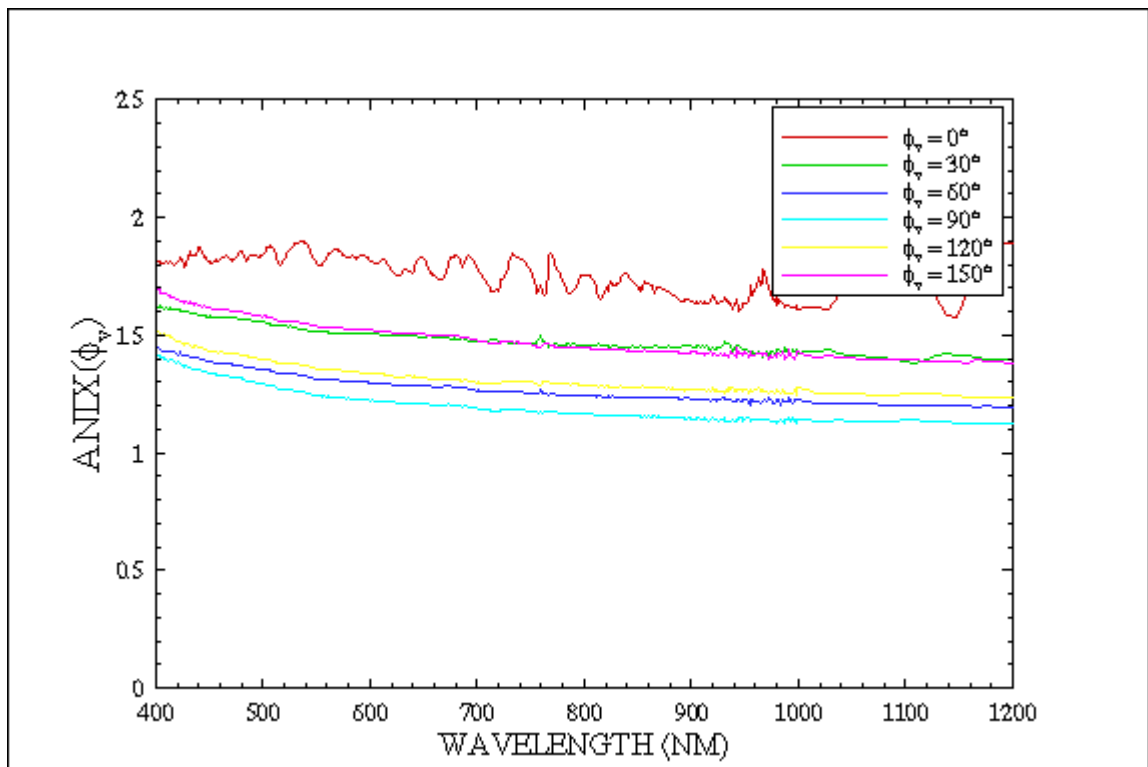


Figure 2-6: Anisotropy in different azimuth planes in the fallow soil

Mean Anisotropic Index

One of the goals of this study was comparison of anisotropy of the various data sets. The Anisotropy Index was found to be the most suitable parameter for this purpose. However, hyperspectral data analysis is a complicated task because of the high dimensionality. Thus to simplify the analysis a new term was developed, the mean anisotropic index. Definition: The mean anisotropic index is an average of the ANIX values over a given range of the spectrum. Mathematically this can be written as follows:

$$ANIX_{mean} = \frac{\sum_{i=1}^N ANIX(\lambda_i)}{N}, \quad (2.10)$$

Hemispherical Reflectance (ρ)

Hemispherical reflectance, also known as surface albedo is crucial for studies on climatology. It is also used in building radiative transfer models, numerical weather prediction models and global climate models [9]. In the past, researchers used the nadir reflectance as a substitute for the surface albedo because the available sensors had a single view direction. However, further studies have demonstrated that using the nadir reflectance as the albedo can result in errors as high as 45-50%. The goal behind calculating the albedo (hemispherical reflectance) in this study was to understand the overall reflectivity of the soils and compare them.

Definition: Hemispherical Reflectance is the ratio of the radiant energy emitted from a surface in all directions to the irradiance energy from a collimated source, incident from a specific direction [3]. Mathematically it can be stated as follows:

$$\rho(\lambda) = \frac{\phi_R(\lambda)}{\phi_I(\lambda)}, \quad (2.11)$$

In equation 2.11 ϕ_R is the total energy reflected from the surface and ϕ_I the total energy illuminating the surface. A highly reflective or scattering surface will have high values of ρ , while an absorptive surface will yield low values of ρ . The maximum and the minimum values possible for ρ are 1 and 0.

Calculation of Hemispherical Reflectance

The BRF is a ratio of the energy reflected in a certain direction. Thus the integration of the BRF values over the complete hemisphere is used to calculate the hemispherical reflectance (equation 2.12). Thus equation 2.11 can be supplemented by equation 2.12. In order to calculate the hemispherical reflectance equation 2.12 is approximated by a numerical integration technique (equation 2.13) as described in [9].

$$\rho(\lambda) \cong \frac{\int_{\phi_v=0}^{2\pi} \int_{\theta_v=0}^{\pi/2} BRF(\theta_v, \phi_v; \theta_i, \phi_i; \lambda) \cdot \cos(\theta_v) \cdot \sin(\theta_v) d\theta_v d\phi_v}{\pi}, \quad (2.12)$$

$$\rho(\lambda) \approx \frac{\sum_{j=1}^N BRF_j(\lambda) \Delta\Omega_j}{\pi}, \quad (2.13)$$

The projected solid angle $\Delta\Omega_j$ of a partition of the 2π steradian solid angle can be calculated using equation 2.14, θ_j varies over all the zenith angles at which measurements are taken. The quantity BRF_j is the average of the reflectance factor measurements taken at the zenith angle θ_j in all the azimuth planes ($\phi_1 \leq \phi_k \leq \phi_N$). The method to calculate BRF_j is given in equation 2.15.

$$\Delta\Omega_j = \pi(\sin^2 \theta_j - \sin^2 \theta_{j-1}), \quad (2.14)$$

$$BRF_j(\lambda) = \frac{\sum_{k=1}^N BRF(\theta_j, \phi_k, \theta_i, \phi_i, \lambda)}{N}, \quad (2.15)$$

CHAPTER III

EXPERIMENTAL DETAILS AND THE GONIOMETER

Introduction and motivation for the SFG

The Sandmeier Field Goniometer (SFG) was built by the Systems Engineering Division, at NASA Ames Research Center, in May 1999. The SFG is based on the design of the Swiss Field Goniometer System (FIGOS). While FIGOS is a semi-automated instrument the SFG is fully computerized. The main purpose behind the construction of the SFG was to build a tool to assist in the research of BRDF phenomenon in various man-made and natural surfaces being conducted by the Commercial Remote Sensing Program (CRSP) at Stennis Space Center, Mississippi.

Technical Specifications of the SFG

Figure 3-1 is a photograph of the SFG and gives an idea of its construction. The goniometer rests on the ground on its azimuth arc. This arc has a diameter of 4 meters. The zenith arc (the vertical semi-circle) is coupled to the azimuth arc. The sensor is mounted onto the zenith arc and its movement, is controlled by a sled.



Figure 3-1: The Sandmeier Field Goniometer

Sensor Details

The sensor used was a GER-3700 spectroradiometer (serial no. 1013). The sensor is placed inside a box, which has a size of 28.6 x 30.5 x 11.4 centimeters and weighs 64 kilograms. The source of power for the sensor is a 12-volt DC gell cell. It records radiance values in the 300-2500 nanometers (nm) part of the spectrum. These radiances are stored as digital numbers. The sensor takes readings in 704 bands; the sampling rate varies with the wavelength. It is 1.5 nm from 300-1050 nm, 6.5 nm from 1050-1900 nm and 9.5 nm from 1900-2500 nm. The data acquisition time for a single view position is 50 milliseconds or higher, which can be selected by the operator. Although the actual time between two successive readings is about 5 to 6 seconds because of the overhead

involved in moving the sensor unit from one viewing position to another on the zenith arc. The sensor has a 2° field-of-view, thus at nadir the field-of-view of the ground target is only 10.5 square centimeters.

Operation

The goniometer is located over the target in such a way that it is at the center of the azimuth arc. The sensor (mounted on the zenith arc) is made to point to the goniometer's horizontal center from any position. The viewing distance is maintained a constant at 2 meters. Figure 3-2 illustrates the sampling scheme for the goniometer from the top view. The target lies at the center of the concentric circles. Each circle represents the zenith angle between the sensor and the target. The straight lines are the azimuth angle between the target and the sensor.

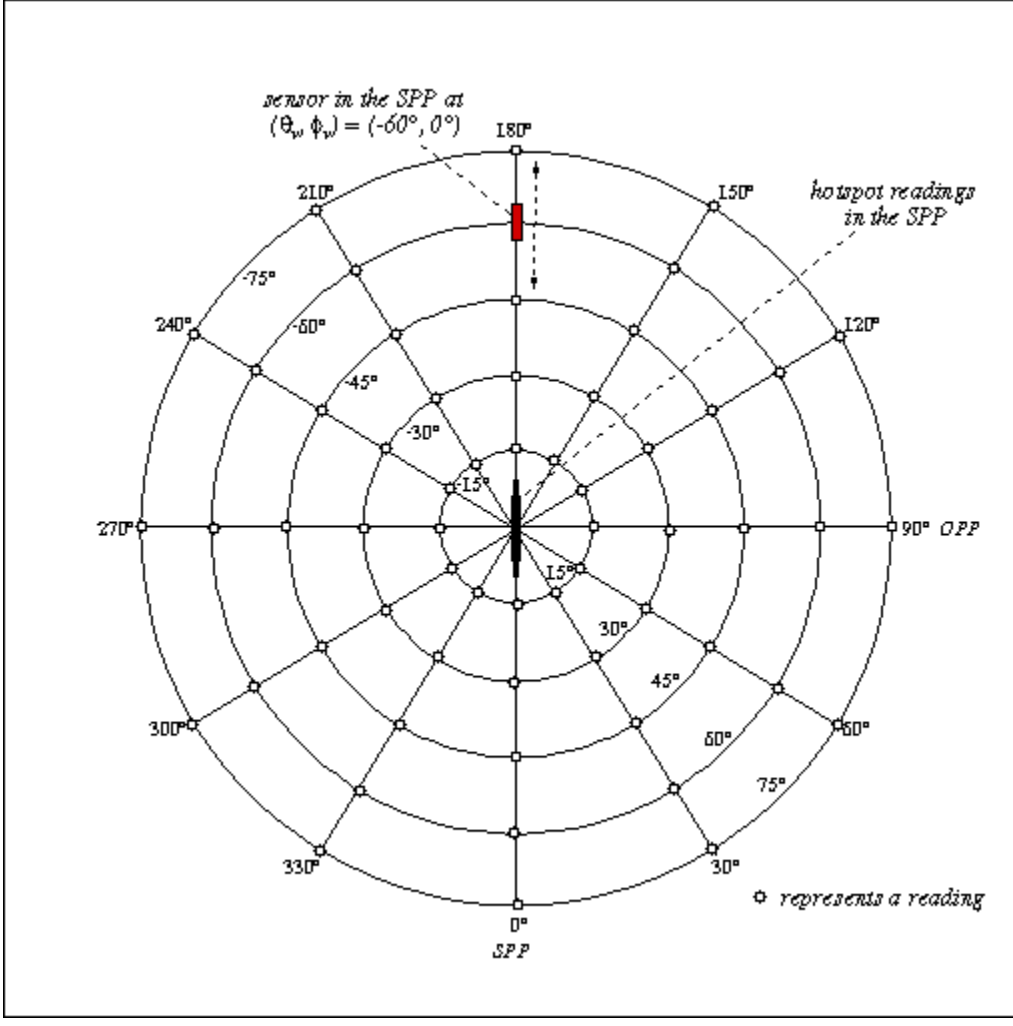


Figure 3-2: Sampling scheme for the goniometer

The SFG is a fully automated instrument controlled by a laptop computer attached to it. The instrument takes measurements at pre-programmed azimuth and zenith angles, starting in the solar principal plane (SPP). The sensor moves over the zenith arc capturing the radiance reflected from the target at regular intervals (the pre-programmed zenith angles). After all the zenith angles in one azimuth plane are covered the zenith arc is rotated around the azimuth arc in order to take readings in the next azimuth plane. This process is repeated until the complete hemisphere around the target is covered.

In our case, the sensor took readings in the 0° azimuth plane from -10° to $+10^\circ$ zenith at an interval of 2° (except at 0° zenith). Then readings were taken at zenith angles -75° to $+75^\circ$ at an interval of 15° . When the sensor was at 0° zenith position (top of the zenith arc) the radiance of a white reference panel was also measured. This was done for each azimuth plane. The azimuth arc was rotated by 30° five times (corresponding to 30, 60, 90, 120 and 150 degrees azimuth plane). In each of these planes measurements were taken from -75° to $+75^\circ$ zenith angle at a regular interval of 15° . No readings were taken at -10 to $+10^\circ$ zenith angle except in the SPP. The readings at negative zenith angles corresponded to readings in the remaining azimuth planes (for example the reading at -75° zenith and 30° azimuth corresponds to a reading at $+75$ zenith and 210 azimuth), thus the complete hemisphere was covered.

Data Log

The radiances were logged in files (ASCII text format) on the hard drive of the computer. Each file corresponds to a unique zenith and azimuth position at which the goniometer took the readings. There are three columns in each file, the first is the wavelength (units: nanometers) at which the reading was taken, the second column is the target radiance (units: $W \cdot cm^2 \cdot nm \cdot sr \cdot 10^{-10}$) and the third column is the radiance of the reference panel. Since measurements at 76 positions were taken during each experiment there are as many data files for each experiment.

Space/Time Tradeoff

The spatial resolution of the instrument poses some challenges to the researcher since a higher sampling resolution (more viewing positions) implies a longer data acquisition time, which causes greater sun movement during the experiment. However, a lower sampling rate could leave out the important reflectance characteristics leading to erroneous conclusions about the BRDF phenomenon.

The sampling strategy for this project, mentioned in the above paragraph led to a data acquisition time of about 9 minutes and restricted the sun movement (zenith and azimuth) within tolerable limits for most of the experiments [please refer to Table 3.2 for the exact sun position for each experiment]. Sandmeier [9] has pointed out that if the sun movement is kept within $\pm 1^\circ$ in the zenith and $\pm 2^\circ$ in the azimuth then the readings are acceptable. The readings were later interpolated to a resolution of 1.2° . Recommendations to expedite the data acquisition process while sustaining the sampling resolution are discussed in Chapter 5.

Site Location and Description

Site Location

The test sites were located at the agricultural farms of Mississippi State University, Mississippi. Three types of bare soils - ridged, disked and fallow were identified to conduct the experiments. Measurements were also taken on zoysia grass. This site was selected only for comparison with published results [9]. The comparison with the published results was crucial in order to proof test the new research instrument (SFG). Table 3.1 lists the GPS locations, elevation above the mean sea level and the date of each experiment.

Table 3.1 Details of the test sites

Site	Latitude (degrees)	Longitude (degrees)	Date	Elevation (above MSL)
Ridged Soil	33.4696514	-88.7796150	11/11/99	80 meters
Zoysia grass	33.4699967	-88.7809728	11/11/99	80 meters
Disked soil	33.4691229	-88.7642917	11/12/99	80 meters
Fallow soil	33.4691903	-88.7646374	11/12/99	80 meters

Site Description

Figures 3.3-3.6 illustrate the surface conditions for each of the test site at the time of the experiment.



Figure 3-3: Ridged Soil



Figure 3-4: Disked Soil



Figure 3-5: Fallow Soil



Figure 3-6: Zoysia Grass

Ridged

The soil at this site (Figure 3-3) is classified as a Marietta fine sandy loam (Fine-loamy, mixed, thermic, siliceous Aquic Fluventic Haplaquepts). The Marietta series consists of moderately well drained, medium acid to moderately alkaline soils. The surface layer is dark grayish-brown fine sandy loam about 15 cm thick.

Four sets of data were taken at the site at four different spots. Figure 3-7 shows the positions of each of the four spots in the ridged soil with respect to the sun. The ridges are 1 meter wide. The 'valley' and the 'shaded' spots lie on the shaded side of the ridge while the 'peak' and the 'sunny' spots are on the illuminated side of the ridge. The particular location of the spots was chosen in order to investigate the effects of shadowing on soil reflectance and anisotropy.

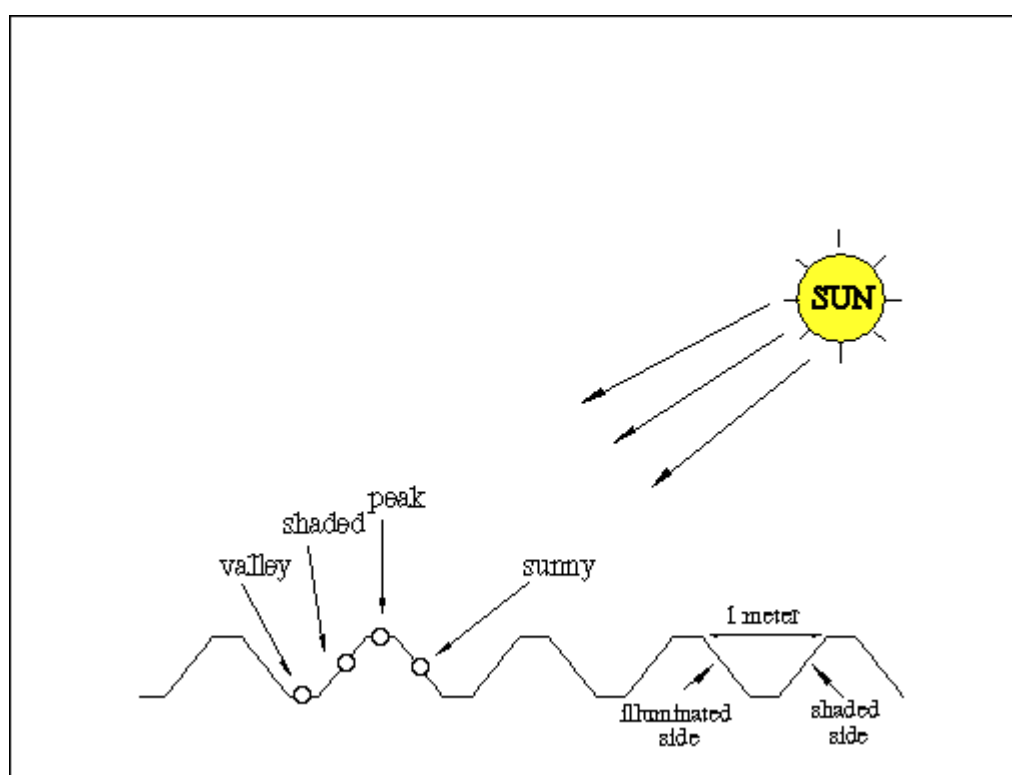


Figure 3-7: Position of the different spots in the ridged soil

Disked and Fallow

The soil at this site (Figure 3-4 and Figure 3-5) is a Leeper silty clay loam (Fine, montmorillonitic, nonacid, thermic Chromudertic Haplaquepts). The Leeper series consists of somewhat poorly drained, medium acid to moderately alkaline soils. The surface layer is very dark grayish-brown silty clay loam, about 13 cm thick. The fallow

and the disked soil differ only by their surface structure. The fallow soil had been lying idle for a long time and was firmly compressed to make a flat and smooth surface. The top surface of this soil is composed of small fine particles.

Four sets of readings were taken in the fallow soil corresponding to different ground conditions - 1) normal dry, 2) a hole in the ground, 3) moist soil (watered lightly) and 4) inundated with water. This was done to observe the impact of soil moisture on surface reflectance.

In order to understand the impact of soil roughness on BRDF, a small region in the fallow soil was ploughed and loosened up before measurement. This made up the disked soil.

Zoysia Grass

This site (Figure 3-6) consisted of short zoysia grass, which was cut uniformly to a length of less than an inch. The same spot was measured in all the three data sets at different times of the day to verify the reproducibility of the SFG. This is explained in detail in Chapter 4.

Experiment Details

Table 3.2 gives the sun positions in the sky on the day of the experiments at the start and the end of each experiment. The sun positions were calculated using a program written by Christopher Gronbeck [2].

Table 3.2 Sun position and timings for each experiment

Site	Start time (CST)*	Azimuth (degrees)	Altitude (degrees)	End time (CST)*	Azimuth (degrees)	Altitude (degrees)
Ridged – valley	11:13 A.M.	8.00	38.78	11:22 A.M.	5.25	39
Ridged – shaded	11:38 A.M.	0.34	39.16	11:47 A.M.	-2.43	39.12
Ridged – peak	12:04 P.M.	-7.63	38.81	12:13 P.M.	-10.35	38.51
Ridged – sunny	12:27 P.M.	-14.53	37.88	12:36 P.M.	-17.16	37.37
Zoysia (1 st morning)	9:24 A.M.	37.71	29.83	9:33 A.M.	35.59	30.95
Zoysia (2 nd morning)	9:47 A.M.	32.15	32.58	9:55 A.M.	30.12	33.44
Zoysia (afternoon)	3:03 P.M.	-51.91	19.65	3:12 P.M.	-53.54	18.15
Disked	12:58 P.M.	-23.26	35.52	1:07 P.M.	-25.7	34.74
Fallow - dry	9:29 A.M.	36.38	30.22	9:37 A.M.	34.47	31.19
Fallow - hole	9:58 A.M.	29.22	33.49	10:07 A.M.	26.86	34.38
Fallow - wet	10:29 A.M.	20.85	36.23	10:38 A.M.	18.3	36.86
Fallow - flooded	11:22 A.M.	5.24	38.72	11:30 A.M.	2.8	38.84

* Daylight Savings Time was in effect at the time of the experiments.

CHAPTER IV

RESULTS

Causes of anisotropy

The general factors responsible for the anisotropy of a target and the measured reflectance are given in Chapter 2. Primarily, the following factors were responsible for anisotropy: 1) sun-sensor geometry, 2) soil roughness and 3) soil moisture.

Shadowing effects

It was mentioned in Chapter 2 that the sun-sensor geometry controls the distribution and amount of shadowing. In the ridged soil the shaded spot is poorly illuminated (see Figure 3-7) since, the sun's rays are blocked by the slope of the soil. The peak and the sunny spot are well illuminated (the contrast in the brightness levels on the two sides of the ridge can be seen in Figure 4-1 or Figure 3-3) since they are on the side of the slope facing the sun. It is not clear from the present ancillary information whether the valley spot was also shaded, but from the reflectance characteristics and other analysis it seems that it received illumination comparable to the un-shaded region. This is discussed in Chapter V.



Figure 4-1: Ridged soil

Figures 4-2 to 4-5 show the reflectance (BRF, equation 2.7) of the four sites in the solar principal plane (SPP) observed at different zenith angles. It is observed that for all the four spots in this soil, the reflectance measured in the backward direction (in the solar direction i.e. the positive zenith angles) are lower compared to that measured in the forward direction (in the opposite direction to the sun represented by negative zenith angles). A common observation for all the four spots in the ridged soil is that the maximum reflectance is observed in the anti-solar direction at an elevation angle of 60° . Reflectance for the positive view angles decreases systematically as the angle is increased, the minimum being observed at $+75^\circ$.

Thus it seems that the ridged soil exhibits specular reflectance to some degree. This is in agreement with Ginneken et al. [1] who have reported that most surfaces in nature demonstrate a mixture of specular and diffuse reflectance. A surface having pure specular reflectance would reflect all the radiation in the forward direction at an angle equal to the modulus of the solar elevation angle. In our case the maximum reflectance is observed in the anti-solar direction at an elevation angle of 60 degrees, while the solar elevation angle at the time of each measurement in the ridged soil was approximately 50 degrees (please see Table 3.2, the elevation and the altitude angles are complimentary). This shift in the hotspot by about 10 degrees can be attributed to the deviation of the ridged soil from a perfect specular reflector. However, unlike a specular reflector the BRF values are scattered over the whole hemisphere.

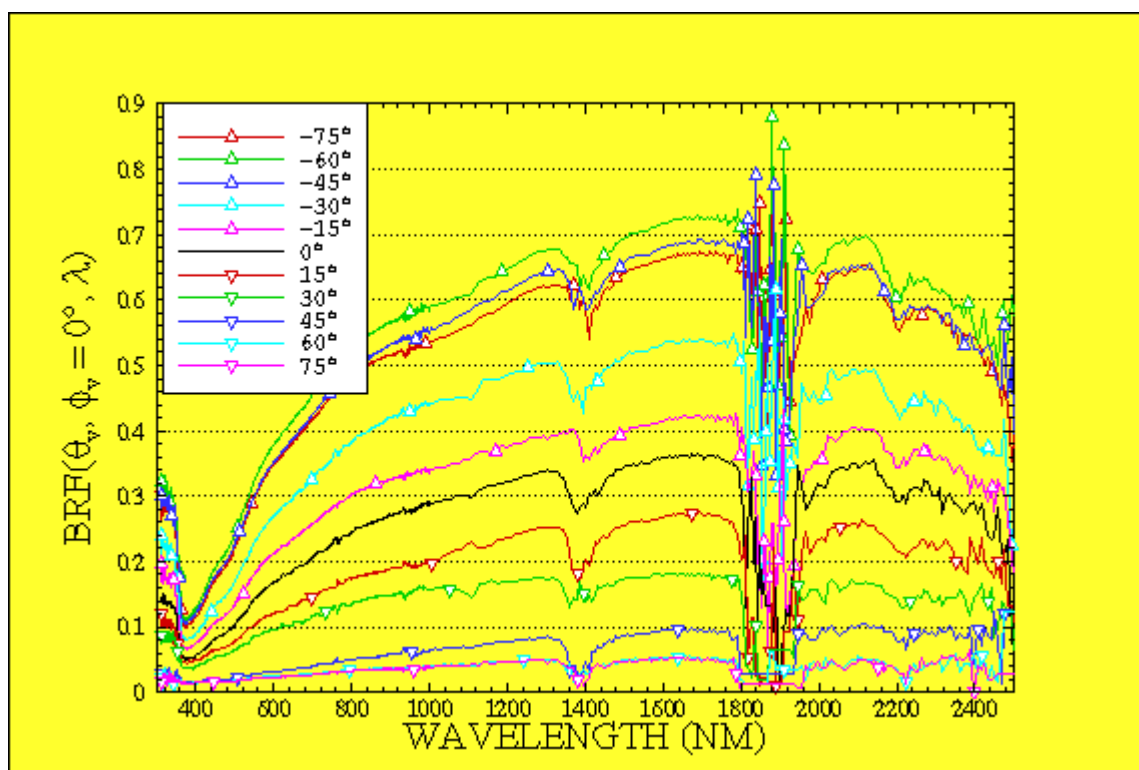


Figure 4-2: Reflectance in the ridged soil (valley spot)

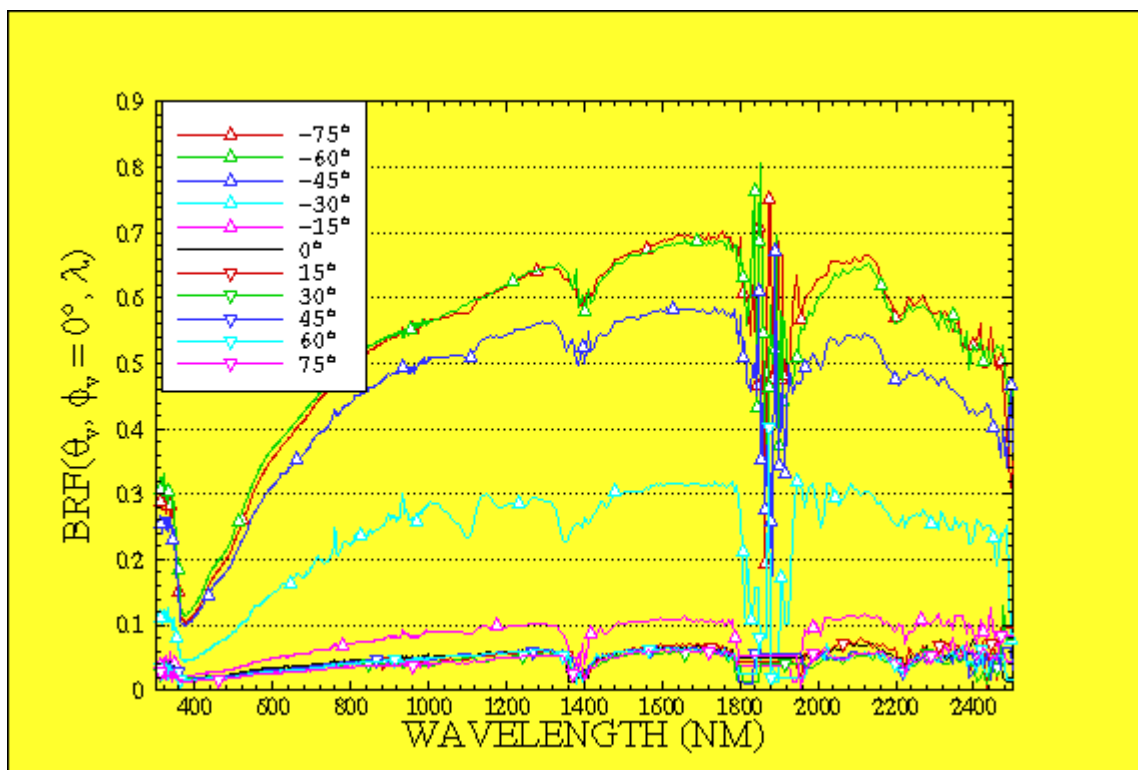


Figure 4-3: Reflectance in the ridged soil (shaded spot)

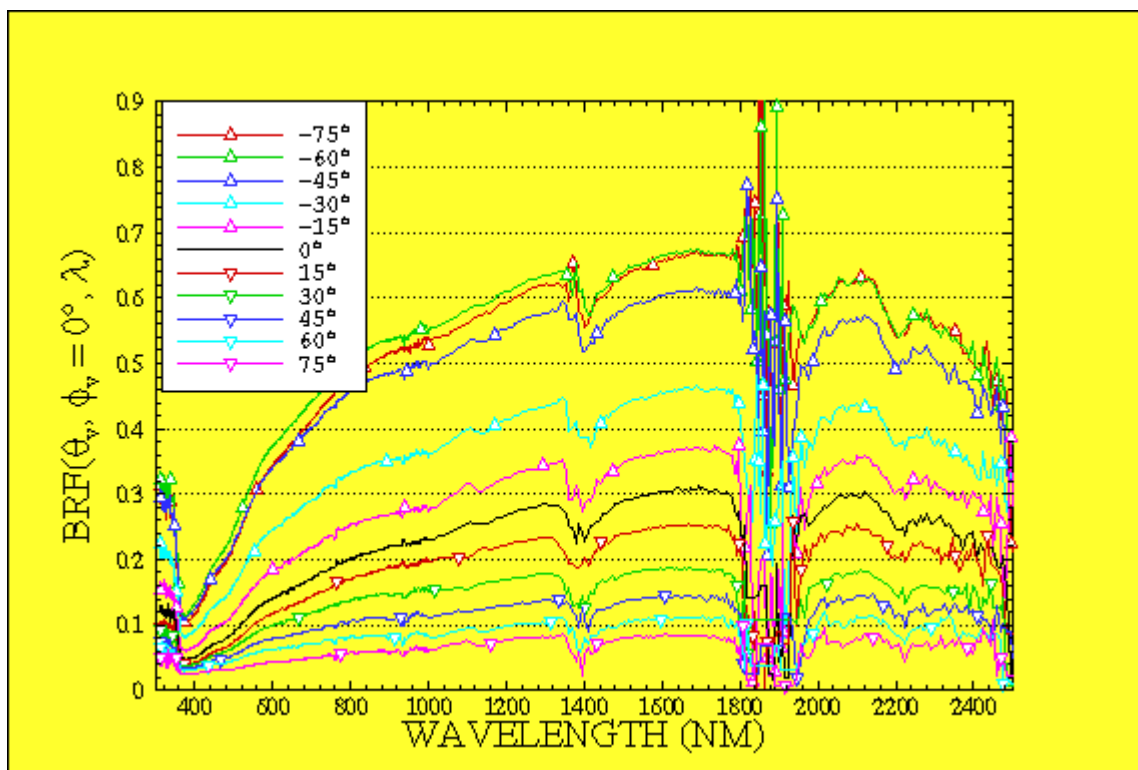


Figure 4-4: Reflectance in the ridged soil (peak spot)

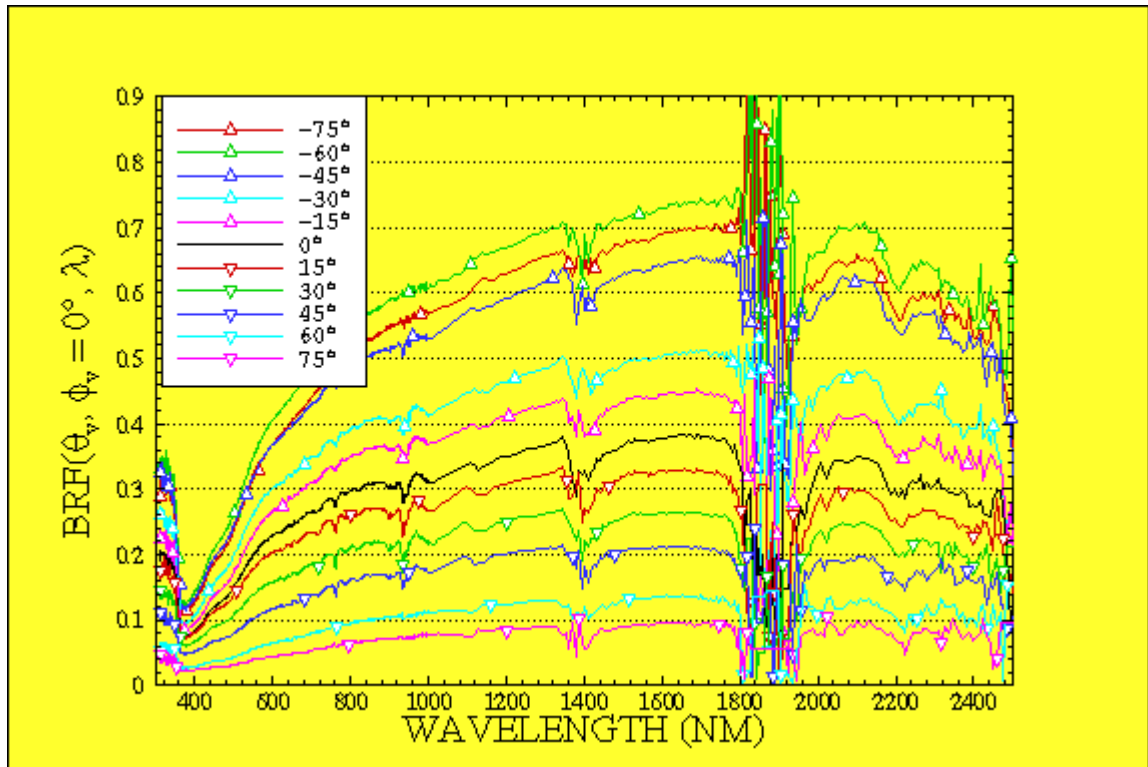


Figure 4-5: Reflectance in the ridged soil (sunny spot)

Comparison of the BRF values of the four spots (valley, shaded, peak and sunny) shows that for the shaded spot the reflectance values are reduced drastically for the backward scattering angles. The anisotropy factor (ANIF, equation 2.8) values in the principal plane (SPP) were also plotted in three-dimensional space as a function of the view zenith angle and the wavelength (figures 4-6 to 4-9). The highest ANIF values for the valley, peak and sunny spot were about a factor of 2. However, the highest ANIF value for the valley spot was more than 11.

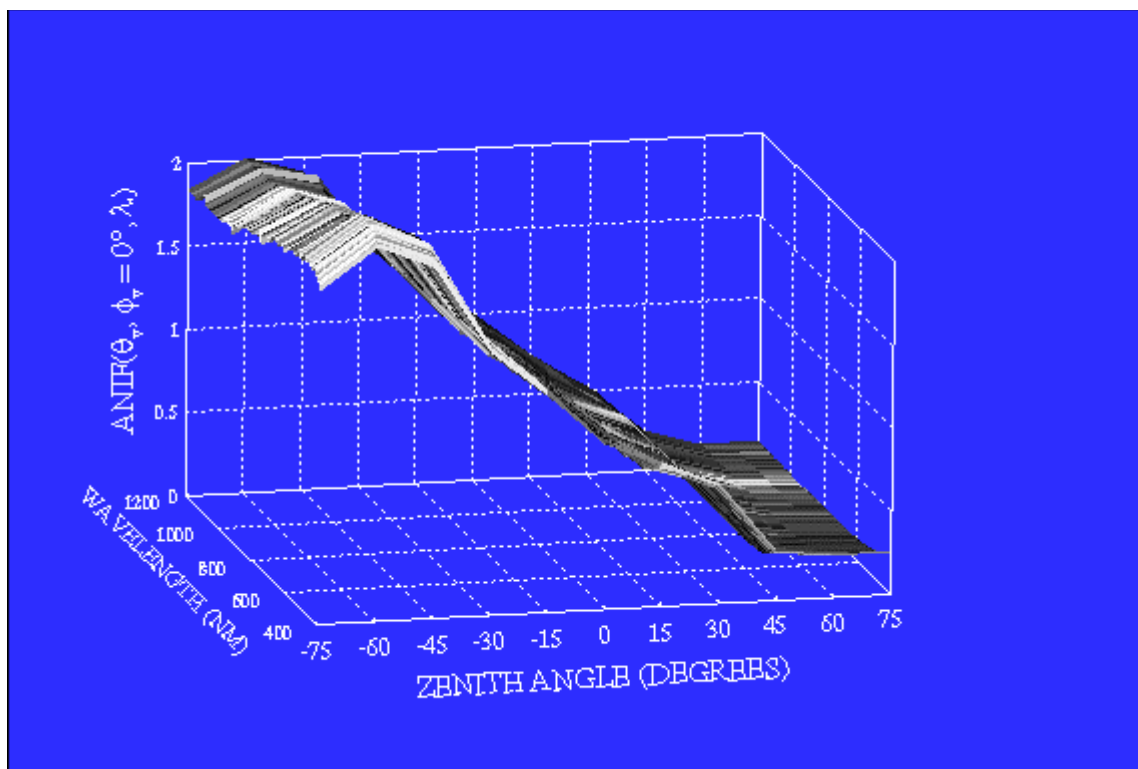


Figure 4-6: Anisotropy in the ridged soil (valley spot)

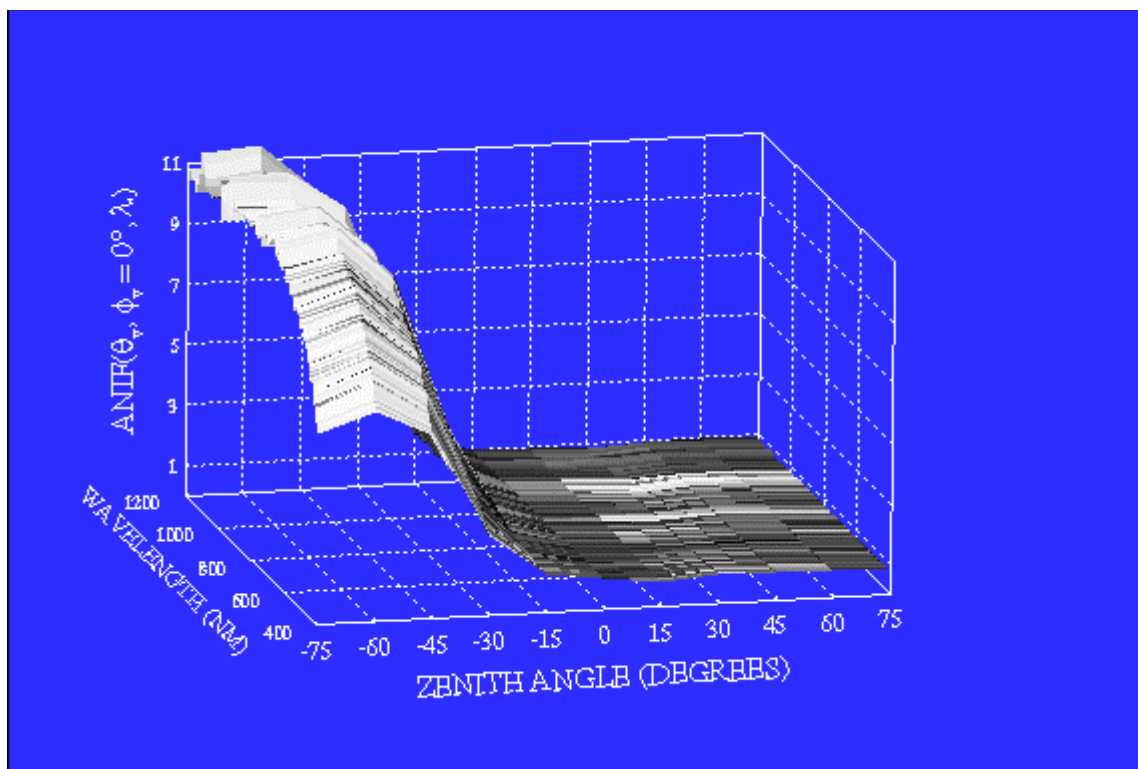


Figure 4-7: Anisotropy in the ridged soil (shaded spot)

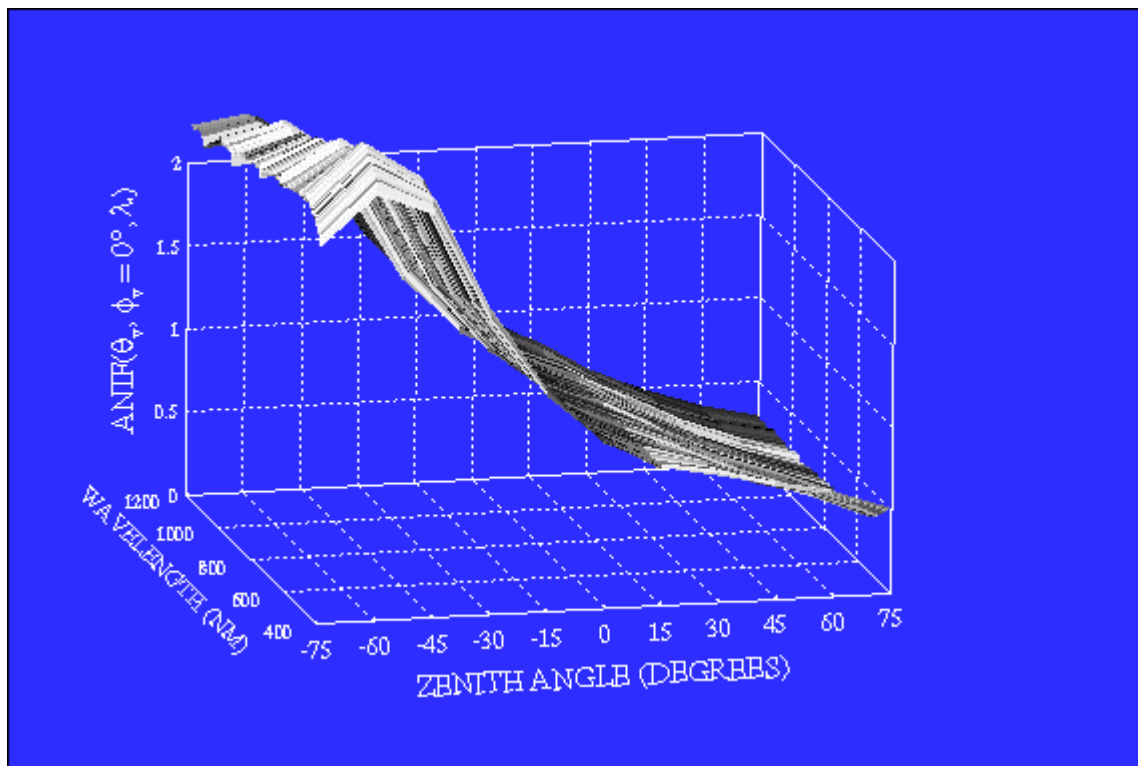


Figure 4-8: Anisotropy in the ridged soil (peak spot)

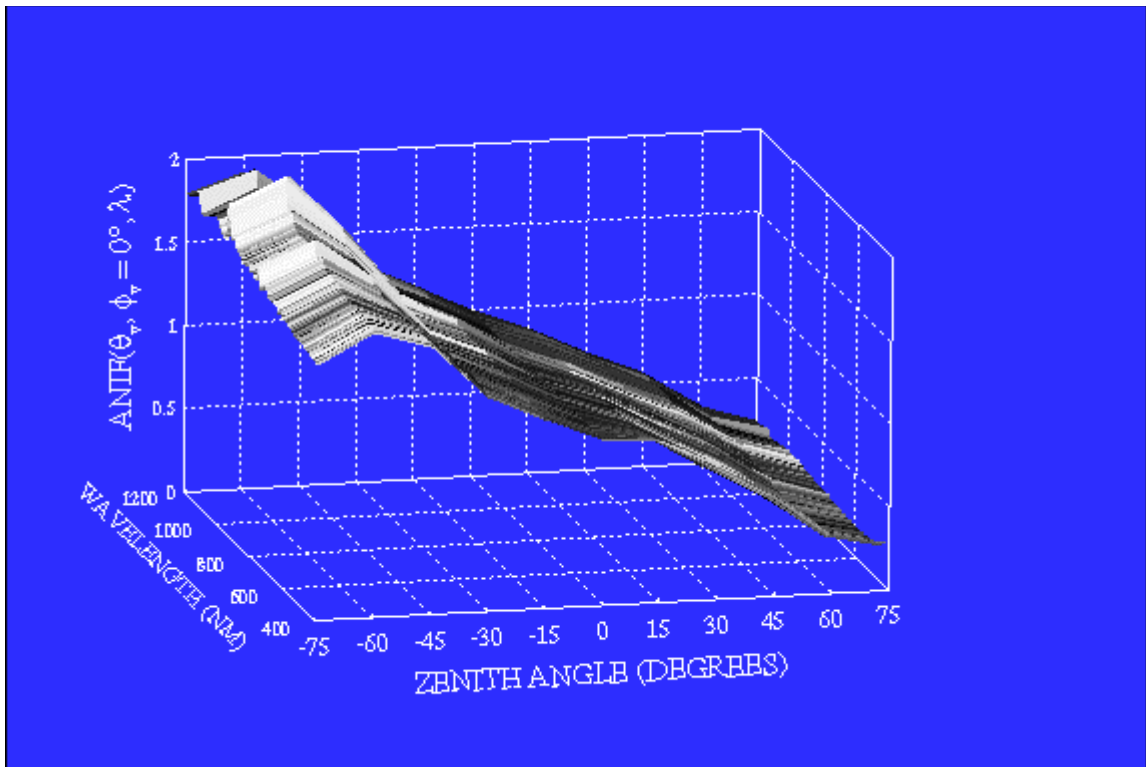


Figure 4-9: Anisotropy in the ridged soil (sunny spot)

The movie `hip_brf.avi` shows the change in the reflectance with the view angle in the solar principal plane for these four spots. BRF values in the backward directions and high forward scattering directions are nearly equal for all the four spots. However, in the shaded spot the BRF values are very low in the range from $[-30^\circ, \dots, 45^\circ]$. The particularly low BRF values in these directions must have been due to blocking of the incident energy by the irregularly shaped particles in the vicinity. Thus shadowing effects play a vital role in determining the reflectance characteristics of a target.

The albedos (approximated by equation 2.15) of these spots are plotted in figure 4-10. As expected the sunny spot has the highest reflectance while the shaded spot has the lowest reflectance. Surprisingly the valley spot has reflectance comparable to the

peak spot. Thus it is confirmed that the valley spot, though located between the ridges, received considerable illumination.

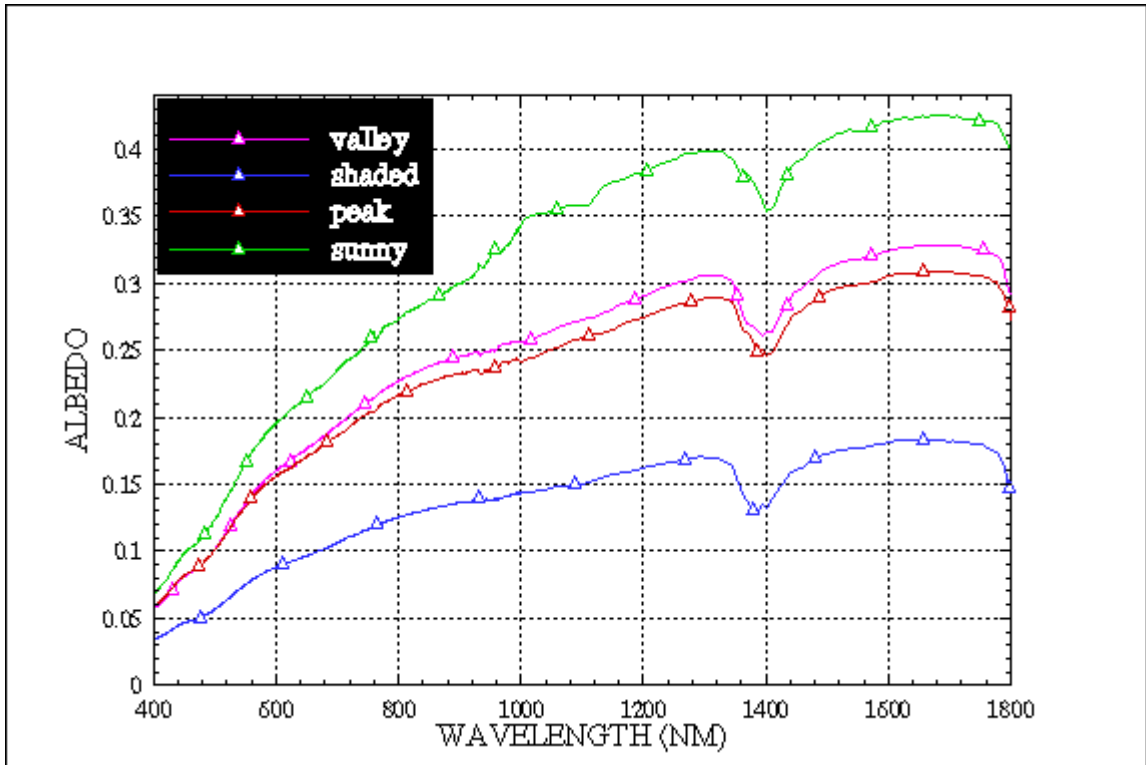


Figure 4-10: Hemispherical reflectance at different spots (ridged soil)

Hip1BRF.mpg, Hip2BRF.mpg, Hip3BRF.mpg and Hip4BRF.mpg are movie clips illustrating the reflectance over the whole hemisphere around the target in the range [400, 1200] nanometers for these spots. Similarly Hip1ANIF.mpg, Hip2ANIF.mpg, Hip3ANIF.mpg and Hip4ANIF.mpg are movie clips illustrating the ANIF distribution. These clips are provided for completeness, similar results can be derived from them.

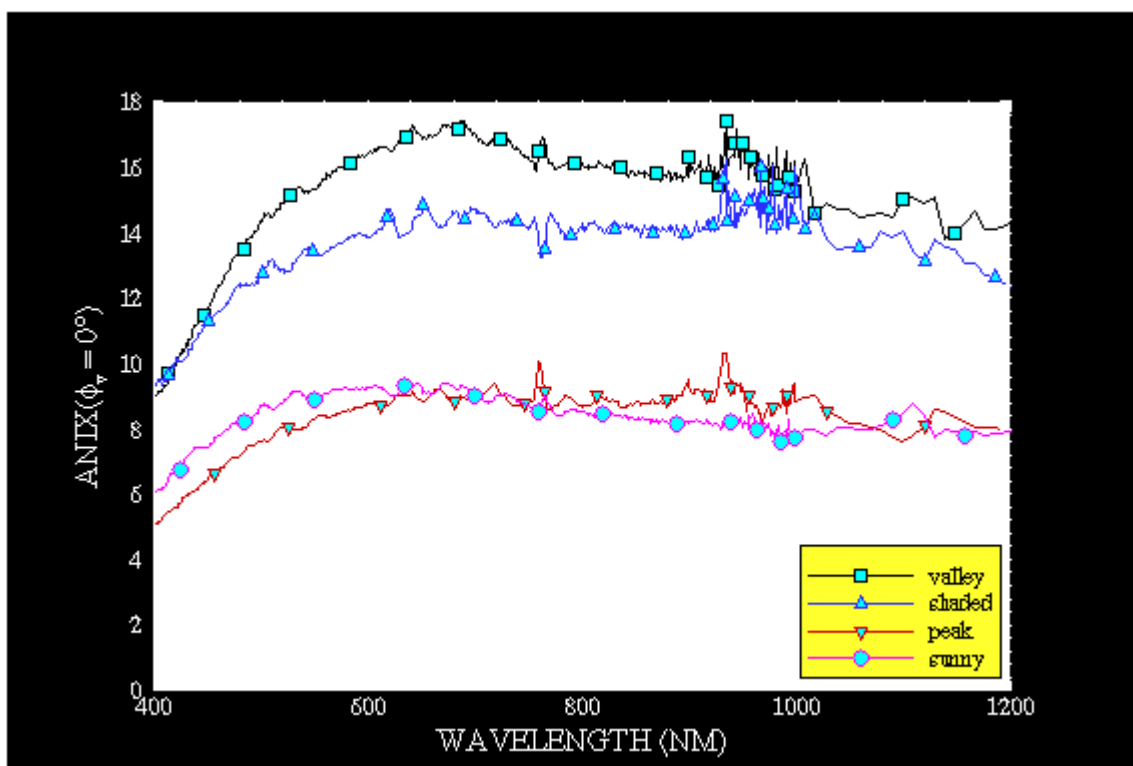


Figure 4-11: Anisotropy in the principal plane for the ridged soil spots

Figure 4-11 gives the ANIX (equation 2.9) values in the SPP for these four spots. The ANIX values in the shaded spot are very high compared to the peak and sunny spots. The ANIX values in valley spot are also higher compared to these two spots.

Soil roughness

In order to observe the effect of soil roughness on reflectance and anisotropy, data sets from the fallow soil and the disked soil were compared. The ridged soil (sunny spot) data set is also used. A description of these soils is given in Chapter 3 in the section titled ‘SITE DESCRIPTION’. The ridged soil and disked soil have big aggregates on the surface, while the fallow soil is compressed and has very small aggregates on the surface.

Effect on Reflectance

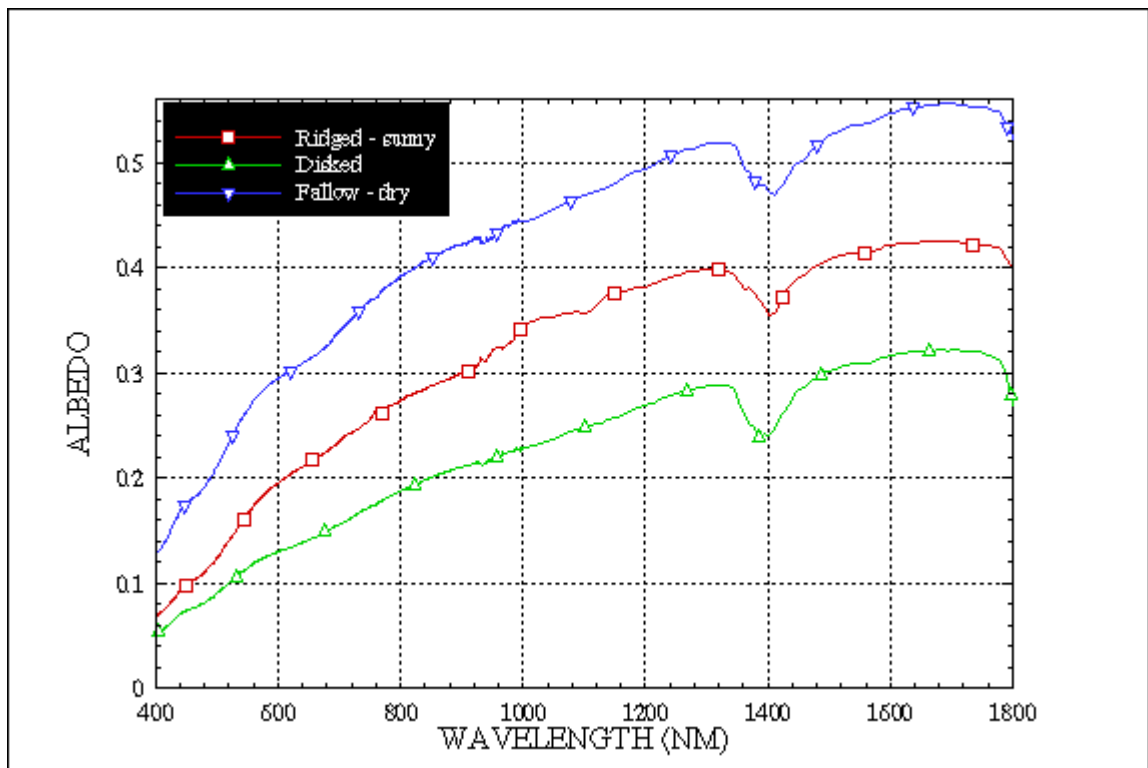


Figure 4-12: Hemispherical reflectance in the three soils

The hemispherical reflectance (albedo) is used to investigate the effect of soil roughness on the reflectance. Figure 4-12 plots the hemispherical reflectance of the three data sets. The albedo of the fallow soil is higher than that of the disked and ridged soil. Thus an increase in the soil roughness leads to a decrease in the reflectance.

Effect on Anisotropy

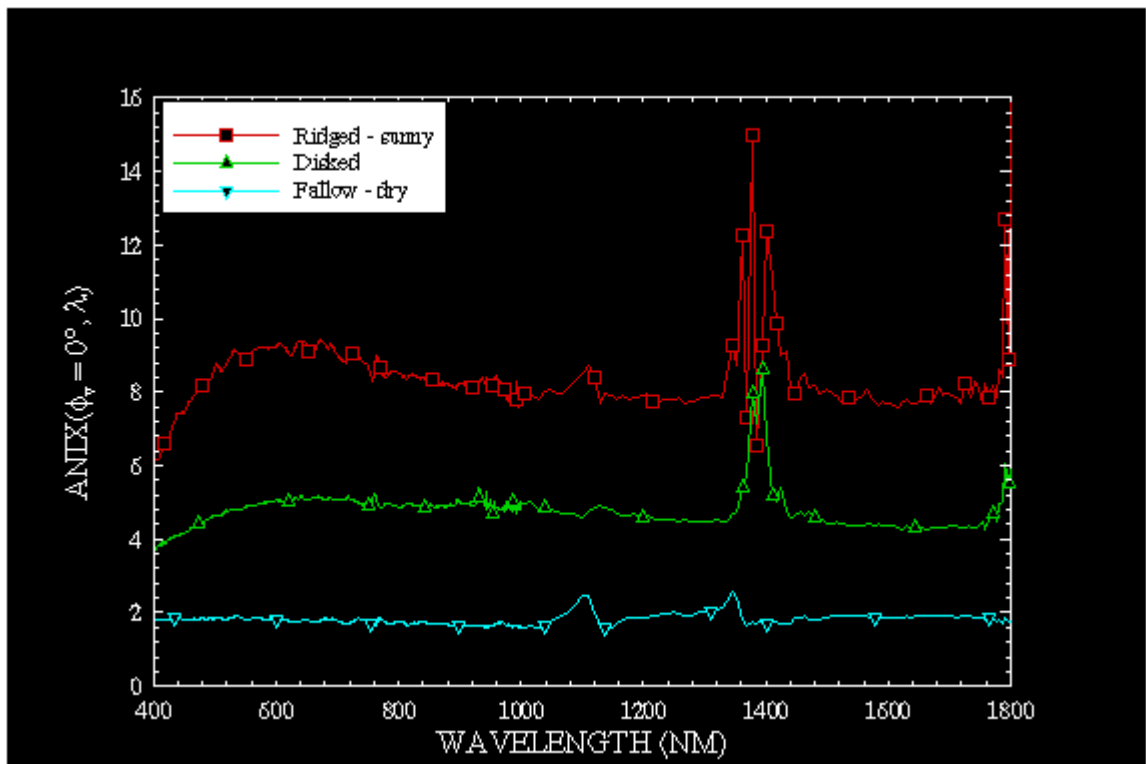


Figure 4-13: Anisotropy indices (SPP) of the three soils

The anisotropy indices (ANIX) of the three data sets measured in the SPP are plotted in Figure 4-13. The ANIX values for the disked soil are more than twice that of the dry fallow soil. Similarly the ridged soil (sunny spot) has a much higher anisotropy compared to the fallow soil. Figures 4-14, 4-15 are ANIF values for the fallow (dry) and disked spots in the principal plane. The anisotropy factor distribution of the fallow soil is quite flat, the maximum being 1.5 while the disked soil has a distribution of about 2.5. The anisotropy of the disked soil is comparable to the anisotropy of the ridged soil (figure 4-9).

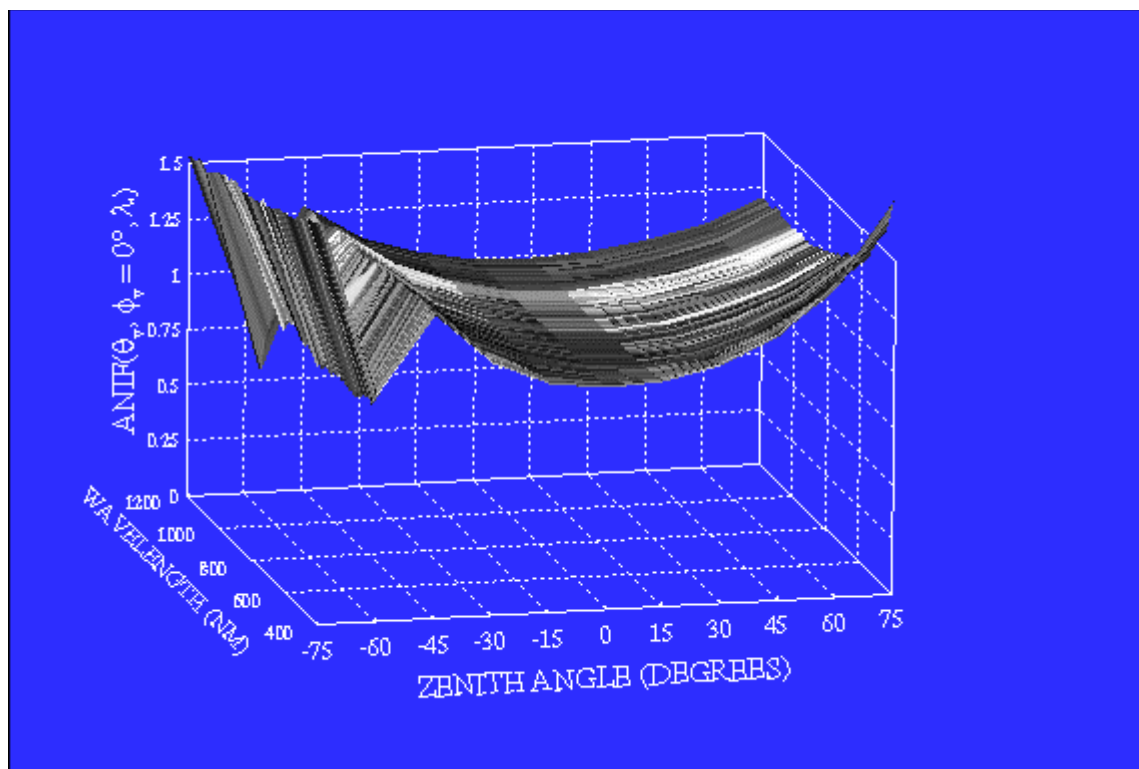


Figure 4-14: Anisotropy in the fallow soil (dry condition)

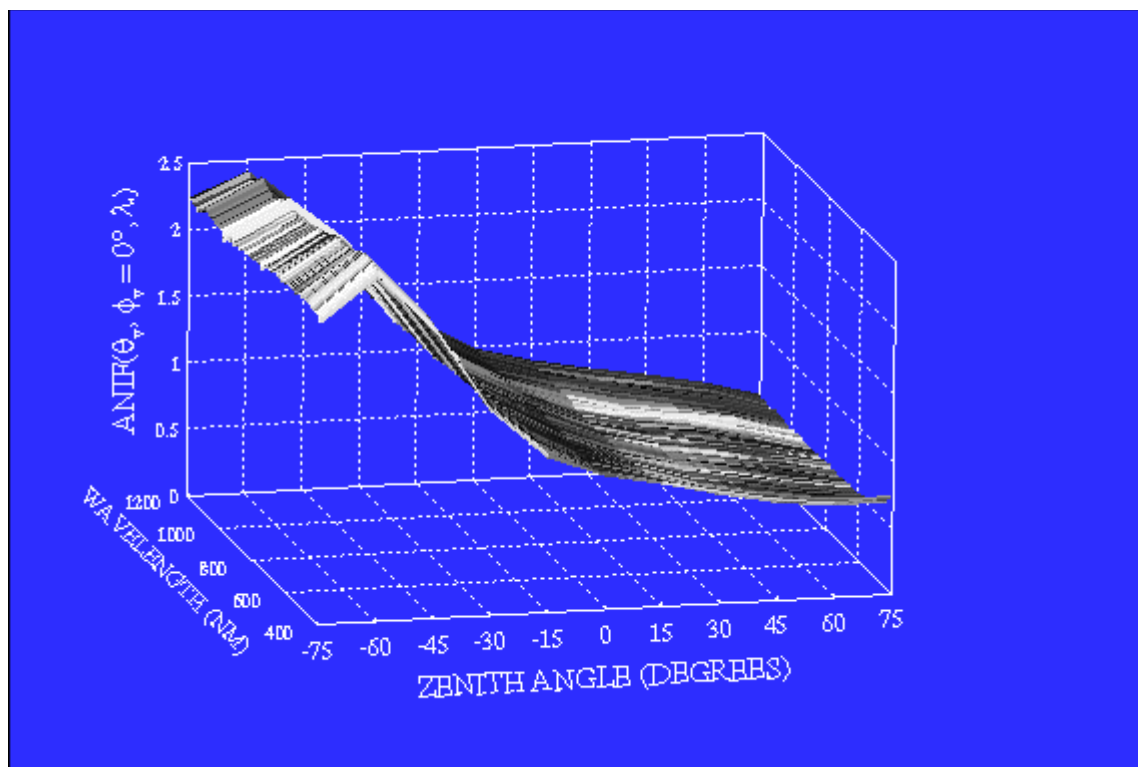


Figure 4-15: Anisotropy in the disked soil

Experiments on the dry fallow soil and the disked soil were conducted within four hours of each other, thus the atmospheric conditions were quite similar. Hence the increase in the anisotropy can be attributed to tilling of the soil. The small particle size and higher particle density in the fallow soil increases multiple scattering, which dominates the single scattering component and causes uniform reflectance in all directions. The solar zenith angle was 55° (please see Table 3.2) at the time when the disked soil data set was collected. The maximum reflectance is observed at about 60° . The relatively big aggregates on this soil scatter in the forward direction into a small angle and thus the single scattering term dominates. This is similar to the phenomenon observed in the ridged soil.

Pac1ANIF.mpg, DiskANIF.mpg and Hip4ANIF.mpg are movie clips corresponding to the fallow (dry), disked and ridged (sunny spot) soil respectively. These clips show the anisotropy distribution of these spots in the hemisphere for the spectral range of [400, 1200] nanometers. The observations are consistent with those observed above.

In the movie clip for the ridged soil (sunny spot) a drastic increase in the ANIF values is observed at about -15° to -30° in the spectral range of [900, 1200] nanometers. A study of all the data sets reveals that the ANIF values at a particular view angle (θ_v, ϕ_v) is relatively independent of the wavelength and shows only minor fluctuations. Thus it is believed that this sudden increase in anisotropy in a part of the spectrum must have been due to noise problems of the sensor.

Soil moisture

The same spot in the fallow soil was measured under four different conditions. These conditions are described in Chapter 3 under 'SITE DESCRIPTION'.

Effect on Reflectance

Figure 4-16 plots the albedo values of the fallow soil measured under these different conditions. It is seen that the reflectance of the soil is reduced by about 50% when water is sprinkled on it (wet condition). However the impact is stronger when the soil is totally flooded with water (flooded) resulting in a drastic decrease in the BRDF values. The reduction in the reflectance is not uniform across the spectral range measured. It is more profound in the NIR region since water absorbs radiation heavily in this part of the spectrum.

Pac1BRF.mpg (dry), Pac2BRF.mpg (hole), Pac3BRF.mpg (wet), and Pac4BRF.mpg (flooded) are movie clips that illustrate the reflectance of the fallow soil under different conditions. A strong backscatter is noticed in the reflectance characteristics of the fallow soil after it is manipulated (hole, wet and flooded).

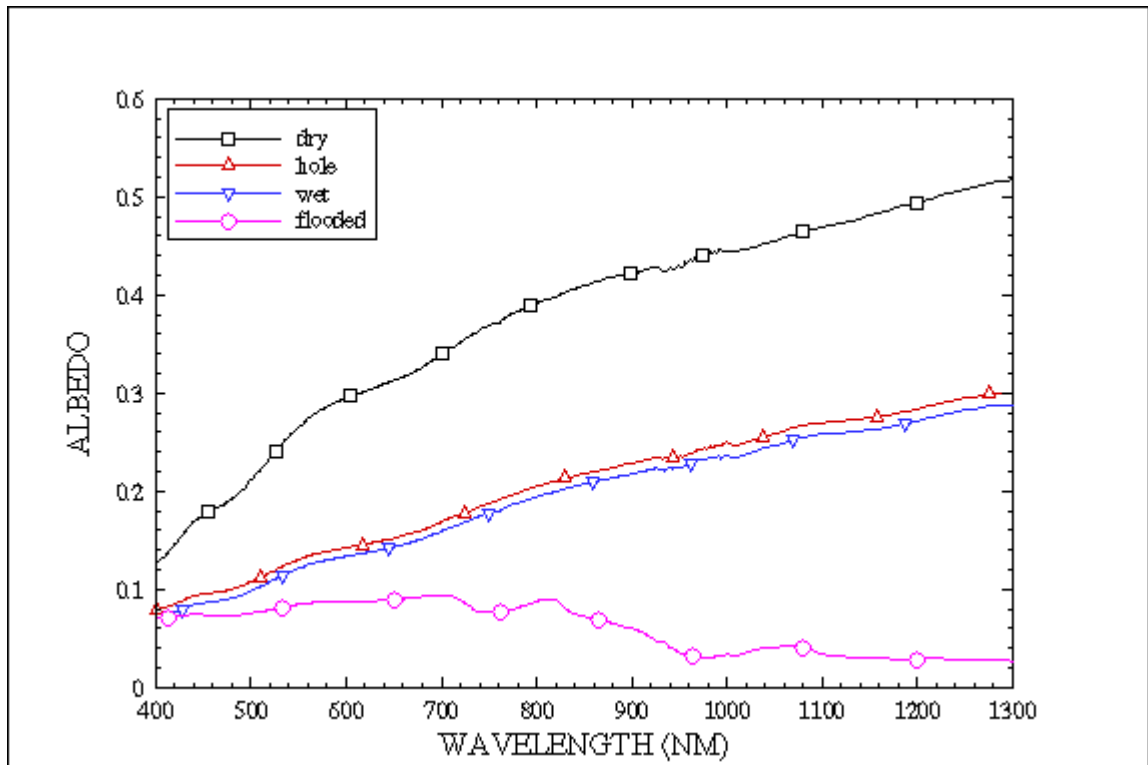


Figure 4-16: Albedo under different conditions

Effect on Anisotropy

Another phenomenon is observed here - the soil anisotropy increases with the increase in water content. Figure 4-17 illustrates the ANIX values obtained from these experiments.

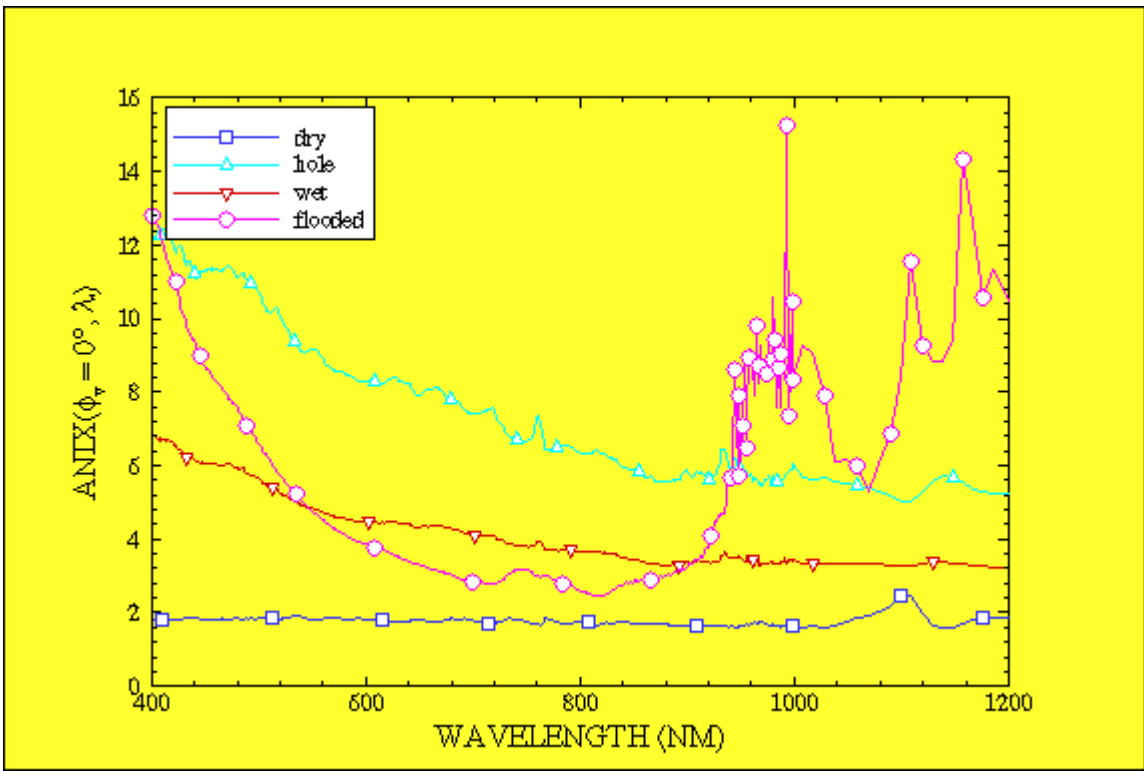


Figure 4-17: ANIX for different conditions in the fallow soil

Figures 4-18 to 4-21 plot the ANIF values of these spots in the principal plane. It is still not clear why the backscatter reflectance increased after soaking the soil with water. Measurements should be taken again under these conditions to see if this happened due to some unusual condition at the time of the experiment. An explanation of this will follow in Chapter 5.

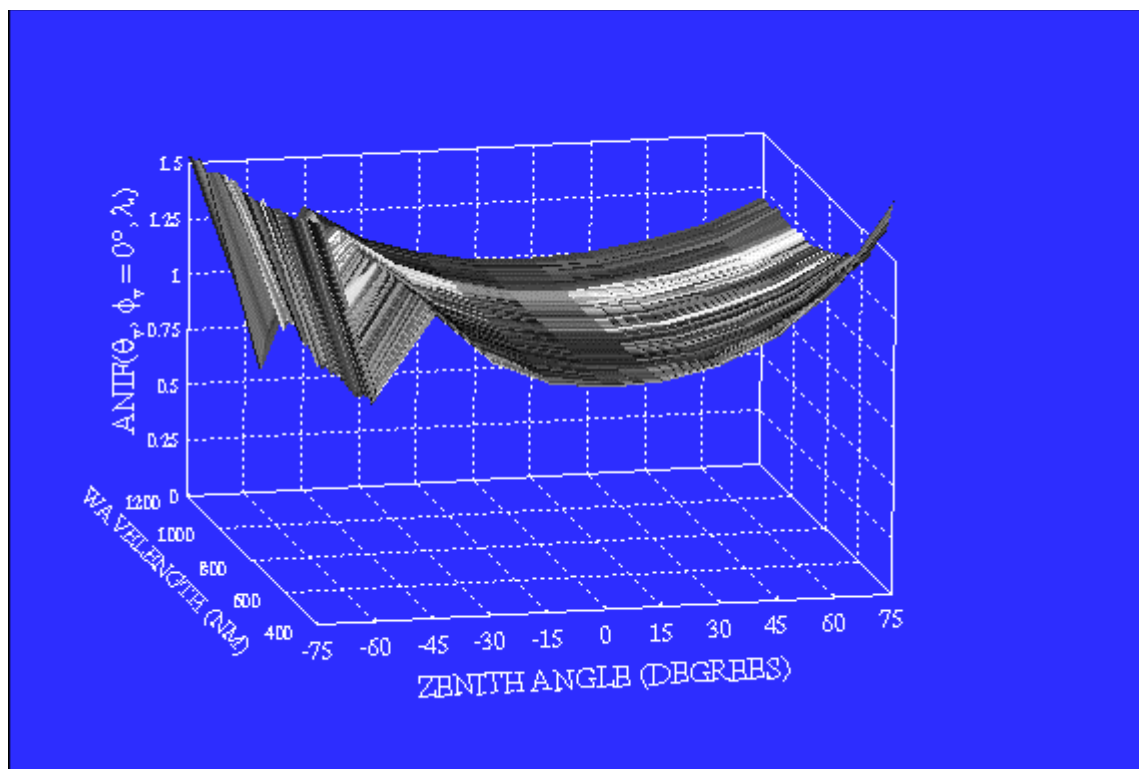


Figure 4-18: Anisotropy in the fallow soil (dry)

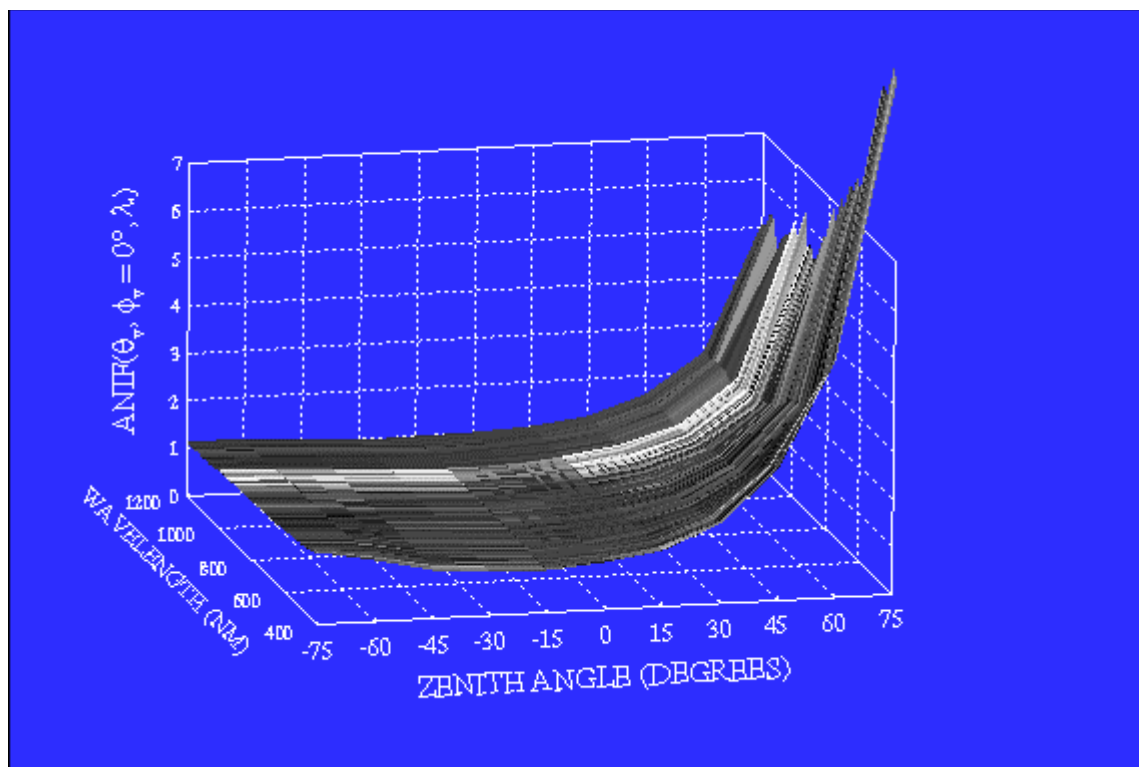


Figure 4-19: Anisotropy in the fallow soil (hole)

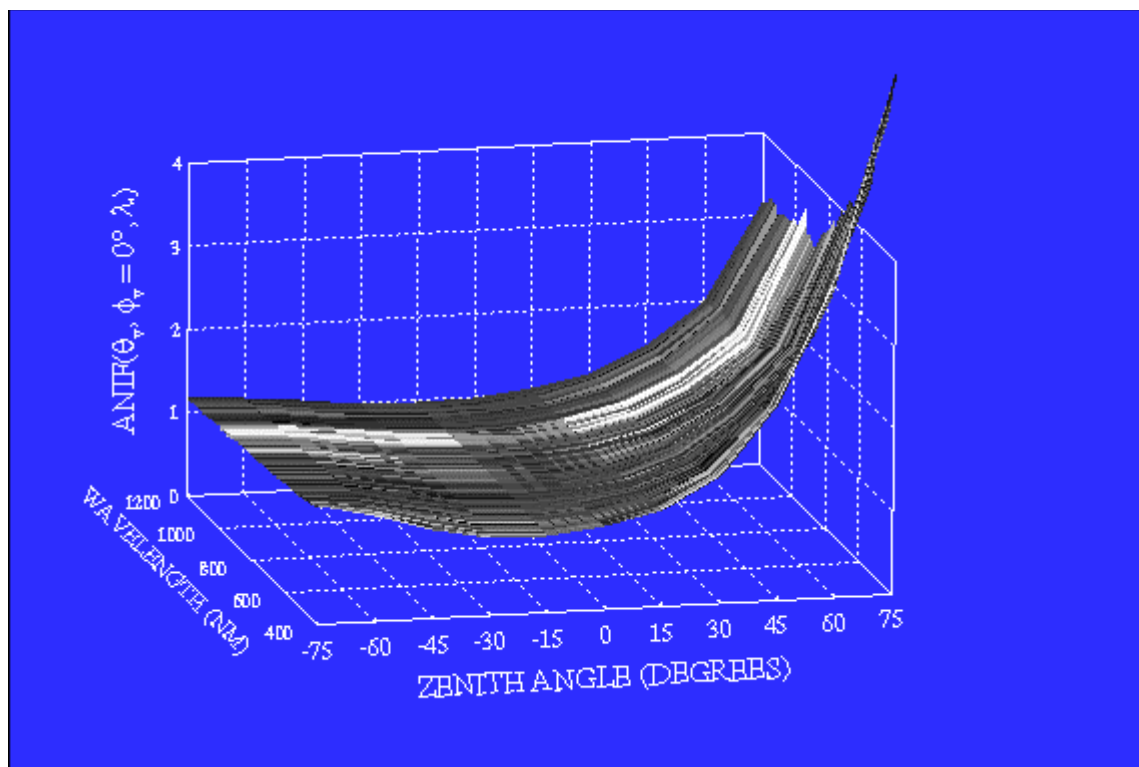


Figure 4-20: Anisotropy in the fallow soil (wet)

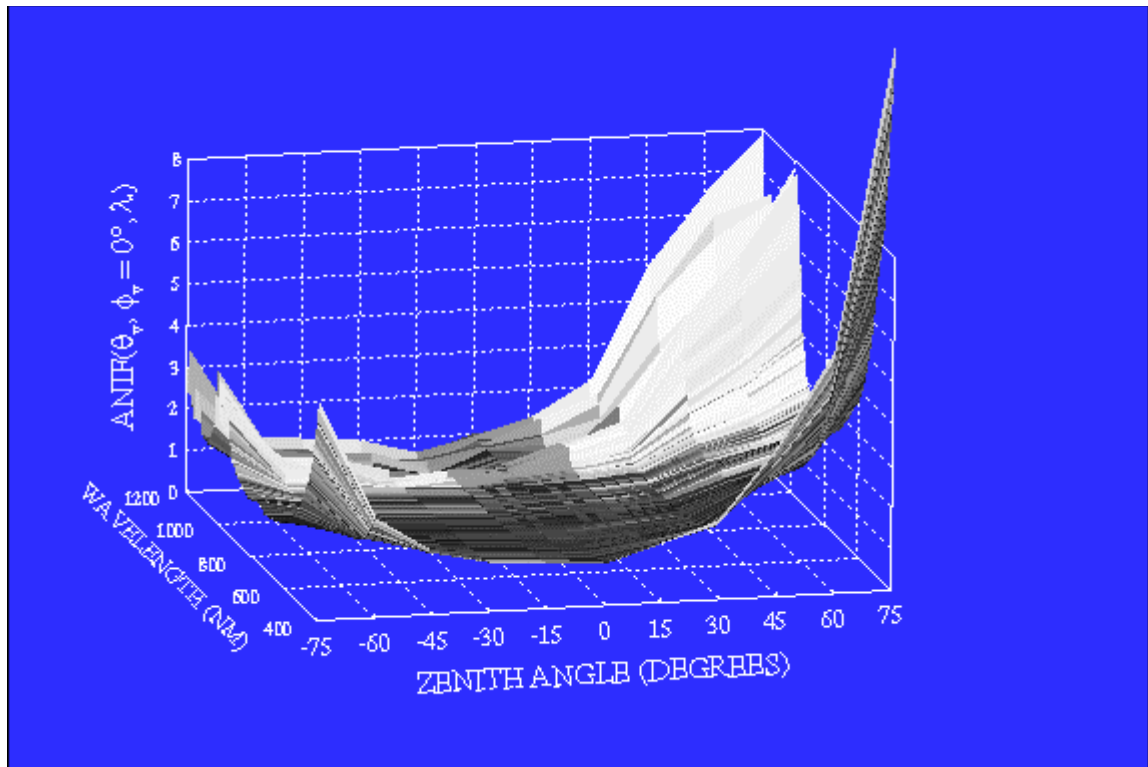


Figure 4-21: Anisotropy in the fallow soil (flooded)

Effect of digging the hole

Digging a hole in the soil reduced the overall reflectance. However, because of a strong backscatter the hotspot is observed in the solar direction at about 60 degrees. Digging a hole exposed the inner soils, which were moist. Thus the reduction in reflectance of this spot can also be attributed to soil moisture.

Zoysia Grass

Generally in plant canopies there are two principal factors affecting BRDF: 1) backscattering and 2) gap effects [13]. However, these factors are almost absent in the zoysia grass data sets. This can be attributed to the short length and the dense structure of the grass.

The incident radiation strikes the grass structure and is multiply scattered within it before emerging out. Thus the out-coming radiance is quite uniform in all directions, which accounts for the low degree of anisotropy in these data sets. Figures 4-22 to 4-24 are plots of the anisotropy (principal plane) of the three data sets measured on the zoysia grass.

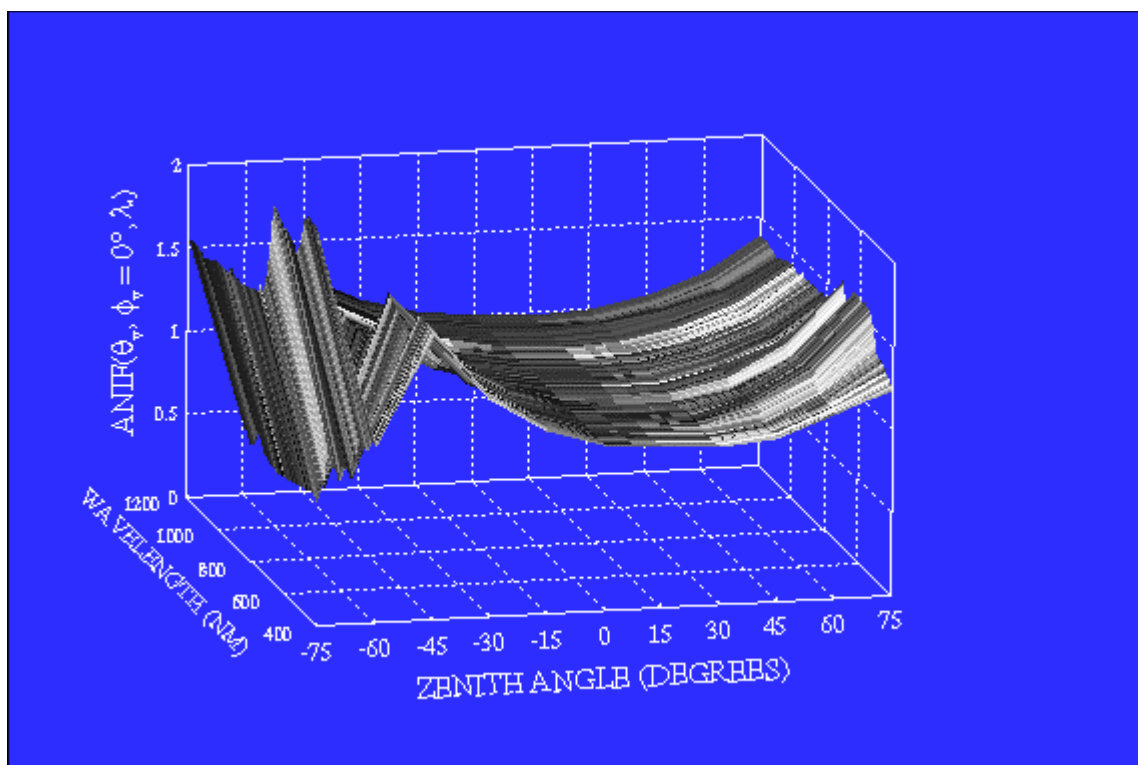


Figure 4-22: Anisotropy in the zoysia grass (9:24 A.M.)

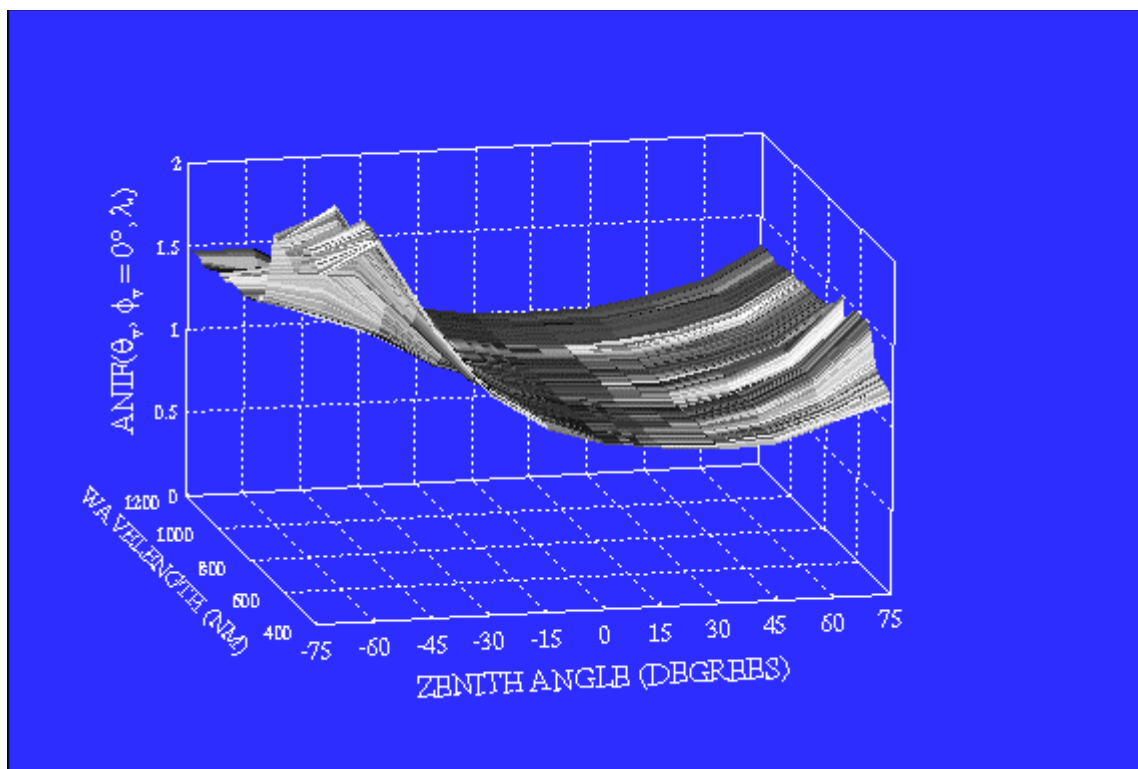


Figure 4-23: Anisotropy in the zoysia grass (9:47 A.M.)

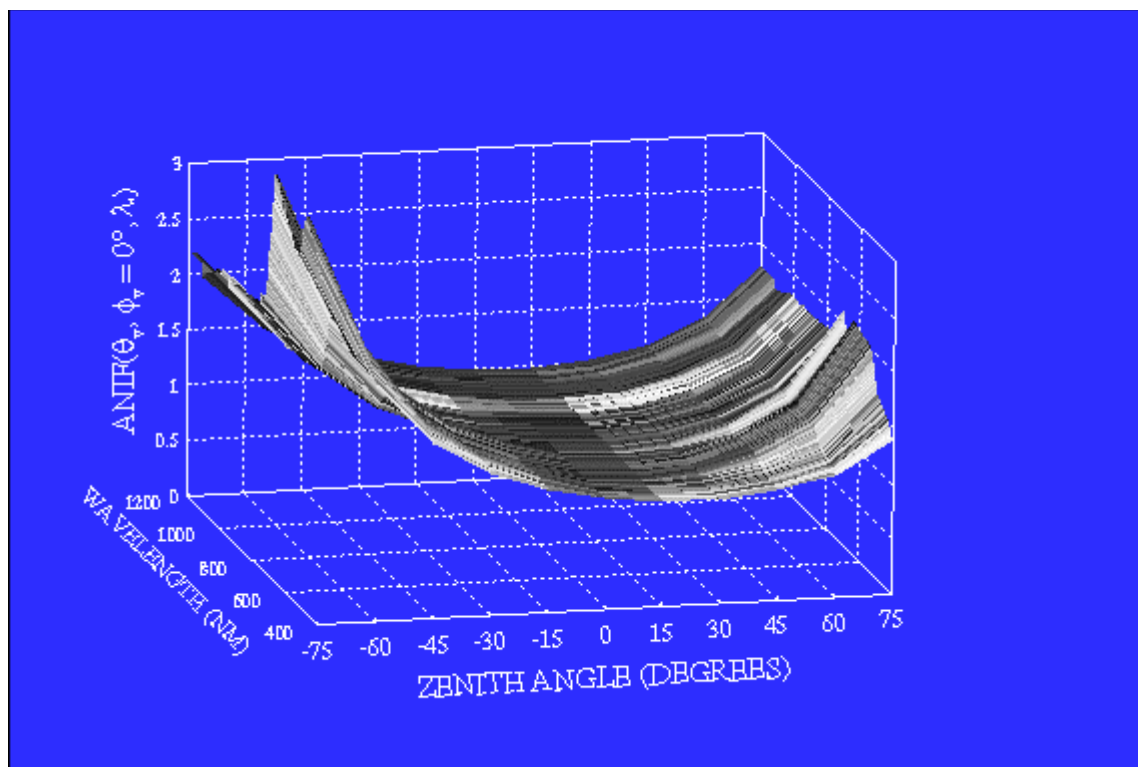


Figure 4-24: Anisotropy in the zoysia grass (3:03 P.M)

Zoy1BRF.mpg, Zoy2BRF.mpg and Zoy3BRF.mpg are movie clips that demonstrate the reflectance of the same spot measured at different times of the day. All the data sets exhibit a bowl-shaped reflectance, with the minimum values observed at nadir. Only in the noon data set (Zoy3BRF.mpg) a strong backscatter is observed at about 15° at a few wavelengths in the range of [900, 1100] nanometers, this can be attributed to noise problems. A drastic increase in the reflectance values after 700 nanometers is also noted, typical of green vegetation.

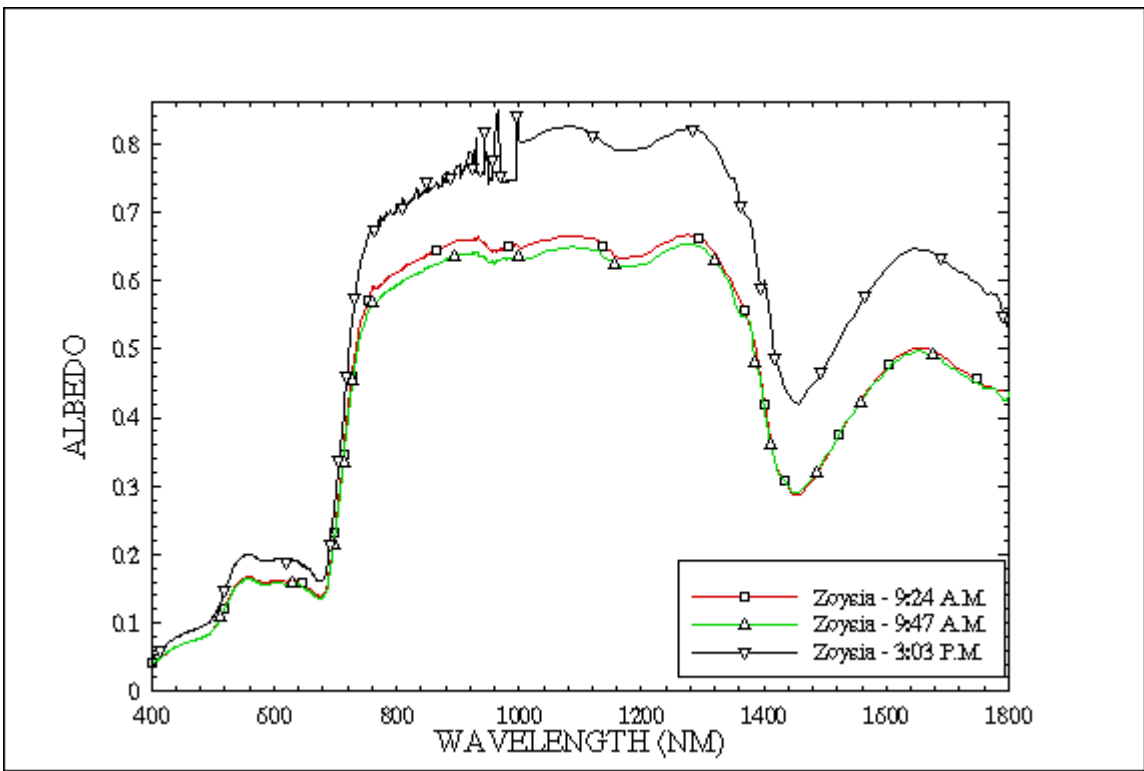


Figure 4-25: Albedo in the zoysia grass

Figure 4-25 shows the albedo values of the grass from the three data sets. The albedo values from the morning data sets match well while those taken in the afternoon are higher. This can be due to the fact that some of the factors that changed between the morning and the noon data sets like: 1) the sun zenith angle changed by about 10 degrees and 2) the physiological condition of the vegetation will be different at different times of the day (moisture content, temperature etc.).

Comparison of Anisotropy of Different Sites

The mean ANIX values (equation 2.10) were calculated for all the sites over the range [400, 1200] nanometers. These are given in Table 4.1. However the mean ANIX values for the sunny spot (ridged soil) data set and the zoysia grass data set collected in the afternoon are higher than they should have been. This is due to noise problems of the sensor. The results from this analysis are quite similar to those observed till now. The ridged soil has the maximum anisotropy. It is confirmed that the valley and the shaded spots have higher anisotropy compared to the peak and the sunny spots. The fallow soil when measured as it is exhibits a very low degree of anisotropy ($ANIX_{mean} = 1.77$). However, adding water to the soil or digging a hole in it increases the anisotropy drastically. The disked soil which had a roughness between the fallow and the ridged soil has a mean ANIX value between the fallow soil and the ridged soil (sunny spot). The zoysia grass has a low anisotropy due to multiple scattering.

Table 4.1 Mean ANIX values ($ANIX_{mean}$)

SITE	$ANIX_{mean}$
Ridged Soil - valley	15.29
Ridged Soil – shaded	13.63
Ridged Soil – sunny	8.51
Ridged Soil – peak	8.41
Fallow Soil - hole	7.8
Fallow Soil - flooded	5.22
Disked Soil	4.79
Fallow Soil - wet	4.33
Zoysia Grass – 9:24 A.M.	3.50
Zoysia Grass – 3:03 P.M.	2.96
Zoysia Grass – 9:47 A.M.	1.97
Fallow Soil – dry	1.77

CHAPTER V

CONCLUSIONS

The experiments principally demonstrate that the soil reflectance is affected by:

- 1) Soil surface structure
- 2) Ground terrain (sun-sensor-target geometry)
- 3) Soil moisture

Soil surface structure

Light scattering, is affected by particle size and interparticle spacing. Light scattered from a surface has two components: 1) singly scattered, this is scattered to the sensor after a single interaction and 2) multiply scattered - this interacts with the surface particles more than once. It has been seen that in brighter surfaces the second component dominates [3] and thus they tend to be more isotropic. Thus we would expect that the dry fallow soil would reflect rather isotropically while the ridged and disked soil would present directional reflectance. Figure 4-13, which plots the ANIX values of the three soils confirms this. Pac1ANIF.mpg, DiskANIF.mpg and Hip4ANIF.mpg are movie clips showing the anisotropy distribution of the fallow, disked and ridged soil (sunny spot) in the hemisphere. These clips clearly show the difference between the flat table anisotropy distribution of the fallow soil compared to the slopes of the ridged and disked soil ANIF distribution.

Ground Terrain

Any change in the terrain features, changes the sun-sensor-target geometry. This in turn causes varying degree of anisotropy for the same type of soil with other factors held constant. This was observed by measuring four spots in the ridged soil. These spots were separated by only a few centimeters but had varying sun-sensor-target geometry.

Soil Moisture

An increase in the soil moisture decreases the reflectance. The effect is more profound in the NIR region. The anisotropy of the soil increased when water was added to it.

Recommendations and future work

It must be mentioned that the experiments conducted had some imperfections, which results in small errors in the recorded reflectance values (BRF). However the conclusions and results recorded here are of general nature and quite correct. These discrepancies were noticed after referring to the literature [12] and [13]. The main causes of error in the BRF values are:

- 1) Non-Lambertian panel and lossy characteristics of the panel
- 2) Presence of diffuse irradiance at the time of the experiments

Errors Due To Non-Lambertian and lossy panel

The BRF is a ratio of the radiance reflected in a particular direction to the radiance reflected by a perfectly Lambertian loss-less panel in the same direction for the same illumination conditions (equation 5.1).

$$BRF(\theta_v, \phi_v; \theta_i, \phi_i; \lambda) = \frac{dL_r(\theta_v, \phi_v; \theta_i, \phi_i; \lambda)}{dL_{ref}(\theta_v, \phi_v; \theta_i, \phi_i; \lambda)}, \quad (5.1)$$

Researchers have reported that the reference panels are not perfectly lambertian. Sandmeier [9] reported errors of the magnitude of 6-8% for Spectralon panels. Thus the term $dL_{ref}(\theta_v, \phi_v; \theta_i, \phi_i; \lambda)$ in equation 5.1 is not the true radiance reflected from a Lambertian panel. It is necessary to quantitatively determine the non-Lambertian characteristics of the spectralon panel used. Thus an additional term $BRF_{ref}(\theta_v, \phi_v; \theta_i, \phi_i; \lambda)$ must be incorporated into equation 5.1 to correct for the non-Lambertianness, this is given by equation 5.2. There are two methods to measure this term: 1) indoor laboratory method [11] and 2) out-door method [5]. Work needs to be done in this direction to quantify this term.

$$BRF(\theta_v, \phi_v; \theta_i, \phi_i; \lambda) = \frac{dL_r(\theta_v, \phi_v; \theta_i, \phi_i; \lambda)}{dL_{ref}(\theta_v, \phi_v; \theta_i, \phi_i; \lambda)} BRF_{ref}(\theta_v, \phi_v; \theta_i, \phi_i; \lambda), \quad (5.2)$$

The reference material is measured only when the sensor is at the top of the zenith arc (nadir) for each azimuth plane. Thus it is sufficient to calculate $BRF_{ref}(0^\circ, 0^\circ; \theta_i, \phi_i; \lambda)$ alone.

Effect of Diffuse Irradiance

In the calculation of the BRF values it was assumed that the target was illuminated only by direct irradiance. In the field both direct and diffuse irradiance are present even on a clear sunny day. If the exact definition of BRDF or BRF is to be followed, it is seen that the denominator is the irradiance from a point source only. Thus the diffuse irradiance must be estimated and subtracted from the total irradiance to get the direct irradiance. There are two methods to quantify the diffuse irradiance - 1) actual measurements and 2) modeling [13].

The first method comprises of first acquiring the BRDF data set for the target surface under total illumination and then acquiring a second data set by obscuring the sun with an opaque panel held at a distance (about 3 meters) from the target so that only diffuse irradiance illuminates the target. Subtracting the second data set from the first data set derives the corrected BRDF values. The mathematical formula for this correction is given by equation 5.3:

$$BRDF(\theta_v, \phi_v; \theta_i, \phi_i; \lambda)^{dir} = \frac{dL_r(\theta_v, \phi_v; \theta_i, \phi_i; \lambda)^{total} - dL_r(\theta_v, \phi_v; \theta_i, \phi_i; \lambda)^{diffuse}}{dL_{ref}(\theta_v, \phi_v; \theta_i, \phi_i; \lambda)^{total} - dL_{ref}(\theta_v, \phi_v; \theta_i, \phi_i; \lambda)^{diffuse}}, \quad (5.3)$$

In the second method the aerosol optical thickness at the time of data acquisition is measured using a sun photometer or any other suitable instrument. This information along with the radiance measured is input to a parametric BRDF model and an iterative procedure is followed. The interested reader may refer to the reference cited above for complete details.

The first method is computationally easy, but time consuming (in terms of field work) while the second method is faster. However neither of these methods can give the true BRDF values since in the first method the sun moves in the zenith and the azimuth directions between the two experiments. Fitting a BRDF model to the data set also involves small amount of errors depending upon the fit between the model and the data set.

Anisotropy as a function of the Surface Roughness

Irons et. al [4] conducted experiments to investigate the effect of surface roughness on anisotropy. They collected three BRDF data sets on the same soil with different tillage methods. This produced surfaces of varying roughness. Table 5.1 lists the

main features of the site at the time of the data acquisition. It must be noted that they used almost similar conditions for all the three cases i.e. the time, the solar zenith angle and the soil moisture content. The only factor, which varied over a wide range (0.08-0.19), was the aerosol optical thickness. The ANIF values in the principal plane (0.75-0.88 μm) were used to compare the anisotropy of these three data sets. They reported that the degree of anisotropy of a soil is saturated after a certain degree of roughness. This means that an increase in the roughness of the soil beyond a certain extent will not increase the anisotropy significantly.

Table 5.1 Details of the experiment (adapted from [4])

Data set	Date	Time of Acquisition (EDT)	Solar Zenith Angle ($^{\circ}$)	Solar Azimuth Angle ($^{\circ}$)	Aerosol Optical Thickness (550 nm)	Soil Moisture Content (%)	Surface Roughness (cm)	Estimated size of the clods (cm)
1	6/30/89	9:51	45	95	0.08	6	2.6 \pm 0.4	4-10
2	8/09/89	9:58	48	104	0.23	6	1.2 \pm 0.2	2-4
3	8/25/89	10:32	45	118	0.19	5	3.9 \pm 0.7	10-25

The data sets acquired by the SFG were also from bare soils having different surface roughness. Thus it was deemed appropriate to compare the anisotropy of the fallow, disked and ridged soil (sunny spot). The plot of the anisotropy in the principal plane of the three data sets is given Figure 5-1. The findings are quite different from those reported in [4]. It is seen that the ANIF values of these data sets differ significantly. The mean ANIX values ($ANIX_{mean}$) of the fallow, disked and ridged soil are 1.77, 4.79 and 8.51. The ANIX values of these three data sets are also plotted in figure 4-13. The

ANIX values of the fallow, disked and ridged soils are in the range of 2, 4 and 8 respectively which are quite different.

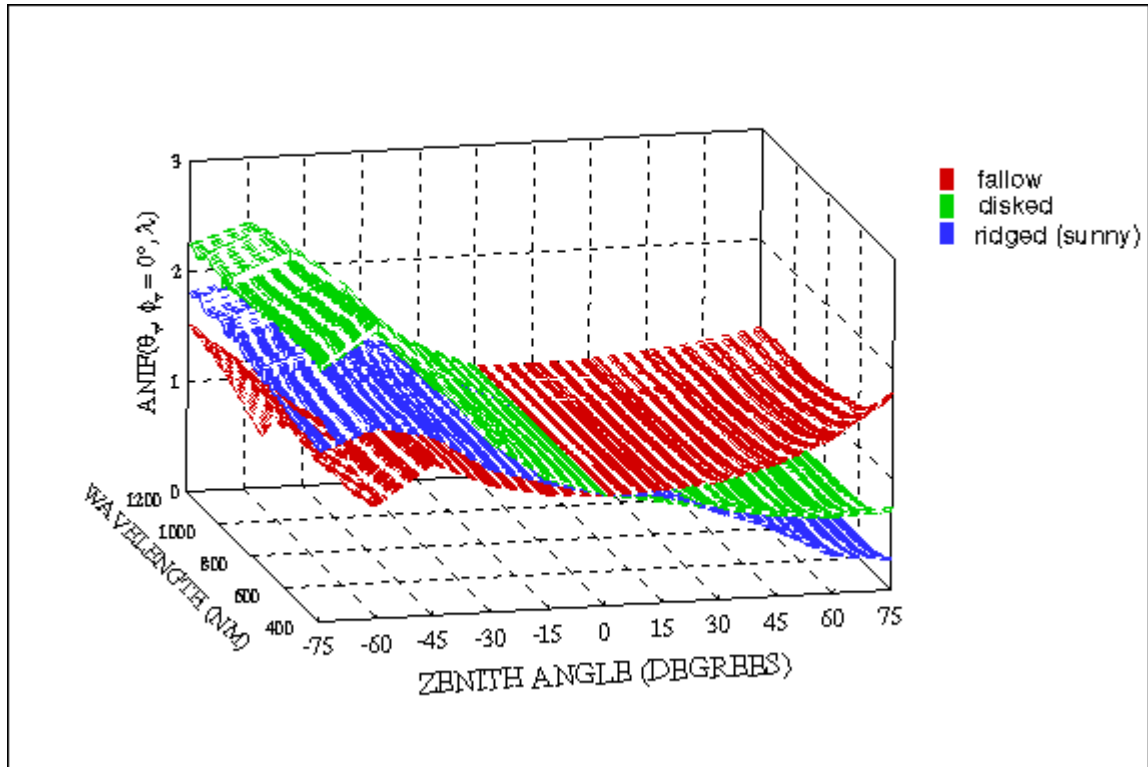


Figure 5-1: Anisotropy (in the SPP) of the three soils

It would be premature to say that the findings in this study are the opposite of those reported in [4]. The experimental setup for the SFG measurements was never designed with the aim of investigating the anisotropy of the soil as a function of the surface roughness. The chemical composition of the fallow and the ridged soil is different. This is a potential factor, which can change the anisotropy.

It is expected that the anisotropy as a function of the surface roughness with other factors remaining constant will saturate at some value of surface roughness. To find this point of surface roughness the following experimental setup (similar to [4]) is suggested:

- 1) The same soil must be tilled to varying amounts of surface roughness and measured before or after data acquisition.
- 2) Readings under conditions of diffuse irradiance (clouds) must be avoided.
- 3) Soil moisture is a factor, which seems to affect the anisotropy (figure 4-17). Thus the soil moisture must be monitored. Data sets with consistent soil moisture values must be used. Readings on or after a rainy day should be avoided.

Irons et. al also state that the data must be collected either at about the same time of the day on different days or if possible on the same day within a small time interval. In the first case the sun position remains almost constant while in the second case the aerosol optical thickness remains nearly the same if there are no drastic changes in the weather. However, it is felt that anisotropy is independent of the illumination angle. This is also a topic of future research.

Multiple Data Sets

It may be possible that one or more of the experiments were affected by some peculiar conditions prevalent at the time of data acquisition, which may lead to wrong conclusions. Thus the experiments must be repeated either for the same spot or on multiple spots on the same soil type to filter out these anomalies and make conclusions based on the average case or the most frequently occurring case. Thus if time and cost permit the site must be re-sampled during the day or over a period of one week. Soil temperatures also vary during the day (low during the morning and high in the afternoon); this can change the BRF values since a hot surface may reflect more energy. In plants, the moisture content may change during the day, which can affect the reflectance values. Repeating the same experiment at different times of the year is highly

recommended since this would help to find any seasonal variations in the BRDF characteristics of the soil [13].

Suggestions to Improve the Data Acquisition Time of the SFG

- 1) Most of the overhead involved in the measurements lies in moving the sensor unit to successive zenith angles on the vertical arc (approximately 5-6 seconds). This could be reduced, by improving the inertial properties of the sensor (weight reduction) a very difficult task.
- 2) The time to locate the zenith arc to a different azimuth plane (by rotating it on the azimuth arc) is also considerable, approximately 16-17 seconds. This also arises from inertial problems of the goniometer.

Readings are taken in 6 azimuth planes, this requires rotating the zenith arc five times and thus an overhead of $17 \times 5 = 85$ seconds. In each azimuth plane the zenith angle must be moved ten times and there are 6 azimuth planes. Thus the overhead in the zenith planes is $6 \times 10 \times 5 + 10 \times 5$ (hotspot readings in the SPP) = 420 seconds. Thus the total overhead for the SFG is $350 + 85$ seconds, a little more than 7 minutes. It would be a major achievement if this were reduced by about 50%. This time could then be utilized to take readings at other view positions resulting in a more accurate representation of the BRDF.

REFERENCES

1. V.B. Ginneken, B.M. Stavridi and J.J. Koenerink, "Diffuse and specular reflectance from rough surfaces", *Applied Optics* vol. 37, pp. 130-139, 1998.
2. C. Gronbeck, <http://www.susdesign.com/sunangle>.
3. B. Hapke, "Bidirectional Reflectance Spectroscopy I Theory", *Journal of Geophysical Research* vol. 86, no.B4, pp. 3039-3054, 1981.
4. J.R. Irons, G.S. Campbell, J.M. Norman, D.W. Graham and W.M. Kovalick, "Prediction and Measurement of Soil Bidirectional Reflectance", *IEEE Transactions on Geoscience and Remote Sensing* vol. 30, no.2, pp. 249-260, 1992.
5. R.D. Jackson, M.S. Moran, P.N. Slater and S.F. Biggar, "Field Calibration of Reference Reflectance Panels", *Remote Sensing of Environment*, vol. 22, pp. 145-158, 1987.
6. R.L. King, <http://www.ece.msstate.edu/~rking/downloads>.
7. R.L. King, P. Pradhan, M.S. Cox and J.W. Jenner, "Comparing Measured Reflectance of Various Soil Surface Roughnesses with a Field Goniometer" *Proceedings of 5th International Conference on Precision Agriculture and Other Precision Resources Management (CD ROM) 2000*.
8. F.E. Nicodemus, "Reflectance Nomenclature and Directional Reflectance and Emissivity" *Applied Optics* vol. 9, no.6, pp. 1474-1475, 1970.
9. A. Nussbaum, *Geometric Optics: An Introduction*, Addison-Wesley Publishing Company.
10. K.J. Ranson, J.R. Irons and C.S.T. Daughtry, "Surface Albedo from Bidirectional Reflectance", *Remote Sensing of Environment* vol. 35 pp. 201-211, 1991.

11. S.R. Sandmeier, E.M. Middleton and D.W. Deering, "Comparing Hyperspectral BRDF Data of Grass Derived from Three Different Laboratory and Field Goniometer Systems", 1998 IEEE International Geoscience and Remote Sensing Symposium Proceedings, ISBN 0-7803-4406-5, IEEE, Piscataway, NJ, 1998a.
12. S.R. Sandmeier, Ch. Müller, B. Hosgood and G. Andreoli, "Sensitivity Analysis and Quality Assessment of Laboratory BRDF Data", Remote Sensing of Environment, vol. 64, no.2, pp. 176-191, 1998b.
13. S.R. Sandmeier, Ch. Müller, B. Hosgood and G. Andreoli, "Physical Mechanisms in Hyperspectral BRDF-Data of Grass and Watercress", Remote Sensing of Environment, submitted, 1998c.
14. S.R. Sandmeier, "Guidelines and Recommendations for the Use of the Sandmeier Field Goniometer", NASA Stennis Space Center, Commercial Remote Sensing Program Office, Verification and Validation Effort, Stennis Space Center, MS, 1999.

APPENDIX A
TABLE OF SYMBOLS

Symbol	Explanation
I	Incident energy
R	Reflected energy
τ	Transmitted energy
α	Absorbed energy
θ_i	Zenith angle of incident ray
ϕ_i	Azimuth angle of incident ray
θ_v	Zenith angle of reflected ray
ϕ_v	Azimuth angle of reflected ray
dL_r	Radiance reflected by the target
dL_{ref}	Radiance reflected by the reference panel
$BRDF$	Bidirectional Reflectance Distribution Function
BRF	Bidirectional Reflectance Factor of the target
$ANIF$	Anisotropy Factor
$ANIX$	Anisotropy Index
$ANIX_{mean}$	Mean Anisotropic Index
ρ	Hemispherical Reflectance
ϕ_R	Total energy reflected from the target
ϕ_I	Total energy illuminating the target
$\Delta\Omega_j$	Projected solid angle of a partition of the 2π steradian solid angle

APPENDIX B

IDL CODE

```

exp_nadir.pro:

;*****;
; Purpose: BATCH PROCESSING OF DATA SETS. ;
; Reads in radiances from GER files and writes BRF, ANIF, ANIX, ;
; RHO etc. ;
; to o/p dat files which can be read in by TECPLOT. ;
; Note: Nadir reflectance is used for normalization of ANIF ;
; values. ;
;*****;
PRO exp_nadir

startTime = SYSTIME(/SECONDS) ; for performance measurement

; base directory for the data
INBASEDIR = $
'/rstc/user1/erc/pushkar/ruff_goniometer_991203/goniometer/SFG Data/'

; location of the data sets
IN_DIR = ['North Farm/Hip1/' , 'North Farm/Hip2/' , $
          'North Farm/Hip3/' , 'North Farm/Hip4/' , $
          'North Farm/Turf1/' , 'North Farm/Turf2/' , $
          'North Farm/Turf3/' , 'Ramsey Bottom/Disked/' , $
          'Ramsey Bottom/Pack1/' , 'Ramsey Bottom/Pack2/' , $
          'Ramsey Bottom/Pack3/' , 'Ramsey Bottom/Pack4/' ]

; directories for o/p files
OUTBASEDIR = '/rstc/user1/erc/pushkar/envipaper1/'
OUT_DIR = ['Hip1/', 'Hip2/', 'Hip3/', 'Hip4/', $
           'Turf1/', 'Turf2/', 'Turf3/', $
           'Disked/', $
           'Pack1/', 'Pack2/', 'Pack3/', 'Pack4/']

; starting names for o/p files
SITES = ['HIP1', 'HIP2', 'HIP3', 'HIP4', $
         'TURF1', 'TURF2', 'TURF3', $
         'DISKED', $
         'PACK1', 'PACK2', 'PACK3', 'PACK4']

name = ''
BASENAME = STRARR(12)

; files containing i/p file name and extensions
file_format_1 = '/rstc/user1/erc/pushkar/envipaper1/GR111199.in'
file_format_2 = '/rstc/user1/erc/pushkar/envipaper1/GR111299.in'

tgtarry = STRARR(76) ; Fixed number of measurements

OPENR, lun, file_format_1, /GET_LUN
READF, lun, name
READF, lun, tgtarry
tgtarry = STRCOMPRESS(tgtarry)
FREE_LUN, lun

; files in North Farm dir. have this name

```



```

BASENAME(0:6) = name

OPENR, lun, file_format_2, /GET_LUN
READF, lun, name
FREE_LUN, lun

; files in Ramsey Bottom dir. have this name
BASENAME(7:11) = name

ext = STRARR(76)          ; file name extension
FOR i = 0, 75 DO BEGIN
    tmp = STR_SEP(tgtarry[i], ' ')
    ext[i] = tmp[0]
ENDFOR

SEP = '.'
infile = STRARR(76)

;*****;
; define the variables ;
;*****;
PTS = 644
h = ' '
wavelength = FLTARR(644)
target      = FLTARR(76, 644)
reference   = FLTARR(76, 644)
;SIG Format (wavel., target rad., referen. rad.)
s          = FLTARR(3, PTS)

BRF        = FLTARR(12, 76, 644)
ANIF       = FLTARR(12, 76, 644)
ANIX       = FLTARR(12, 6, 644)
ANIX_MEAN  = FLTARR(6)
RHO        = FLTARR(12, 644)

; Wavelength index for which the 3-D polar plot is created
INDEX = 457      ; 1050 nm

;*****;
; ;
;          START PROCESSING THE DATA SETS ;
; ;
;*****;
; K - the no. of data sets
FOR K = 0, 11 DO BEGIN

FOR i = 0, 75 DO BEGIN
    infile[i] = INBASEDIR+IN_DIR[K]+BASENAME[K]+SEP+ext[i]
ENDFOR

;*****;
; ;
;          read in the data files ;
; ;
;*****;

```

```

FOR J = 0, 75 DO BEGIN

    OPENR,lun,infile[J],/GET_LUN           ; read one file at a time
    FOR i = 0, 11 DO BEGIN
        READF, lun, h                     ; skip header
    ENDFOR
    READF,lun,s
    wavelength = s(0,*)
    target(J, *) = s(1,*)
    reference(J, *) = s(2,*)
    FREE_LUN, lun

ENDFOR

;*****;
; change target-reference reading reln.ship ;
;*****;
FOR J = 10, 20 DO BEGIN
    IF(J NE 16) THEN BEGIN
        reference(J, *) = reference(16, *)
    ENDIF
ENDFOR

FOR J = 21, 31 DO BEGIN
    IF(J NE 27) THEN BEGIN
        reference(J, *) = reference(27, *)
    ENDIF
ENDFOR

FOR J = 32, 42 DO BEGIN
    IF(J NE 38) THEN BEGIN
        reference(J, *) = reference(38, *)
    ENDIF
ENDFOR

FOR J = 43, 53 DO BEGIN
    IF(J NE 49) THEN BEGIN
        reference(J, *) = reference(49, *)
    ENDIF
ENDFOR

FOR J = 54, 64 DO BEGIN
    IF(J NE 60) THEN BEGIN
        reference(J, *) = reference(60, *)
    ENDIF
ENDFOR

FOR J = 65, 75 DO BEGIN
    IF(J NE 71) THEN BEGIN
        reference(J, *) = reference(71, *)
    ENDIF
ENDFOR

;*****;
;
;

```

```

;               replace readings <= 0                               ;
;               (affected by noise)                               ;
;*****;
FOR J = 0, 75 DO BEGIN
  FOR I = 0, 643 DO BEGIN
    IF((target(J, I) LE 0.0) OR (reference(J, I) LE 0.0)) THEN
  BEGIN
    target(J, I) = target(J, (I-1))
    reference(J, I) = reference(J, (I-1))
  ENDIF
  ENDFOR
ENDFOR

; round off 1195 to 1200 nm for convenient labelling in TECPLOT
wavelength(472) = 1200
;*****;
;
;               calculate BRF and ANIF values                     ;
;*****;
BRF(K, *, *) = target/reference ; BRF(K, 15, *) - nadir BRF

FOR J = 0, 75 DO BEGIN
  ANIF(K, J, *) = BRF(K, J, *)/BRF(K, 15, *)
ENDFOR

;*****;
;
;               calculate HEMISPHERICAL REFLECTANCE              ;
;               and write to file                               ;
;*****;
; Calculate the hemispherical reflectance of the surface
; using numerical integration technique as described in
; Ranson et al. (1991)
; BRF(data set no., position, wavelength)

; calculate hemi. reflectance at each wavelength
FOR NO_OF_WAVS = 0, 643 DO BEGIN

theta_j = [ 0.0, 7.5, 22.5, 37.5, 52.5, 67.5, 90.0 ]*(!PI)/180.0

; calculate the projected solid angle of a partition of the
; 2*pi sr angle.
DeltaOhm = FLTARR(7)
FOR J = 1, 6 DO BEGIN
  DeltaOhm(J) = !PI*(sin(theta_j(J))^2.0 - sin(theta_j(J-1))^2.0)
ENDFOR

R_avg = FLTARR(6) ; 11 zenith angles

; 75 degs.
R_avg(5) = (BRF(K, 10, NO_OF_WAVS) + BRF(K, 20, NO_OF_WAVS) + $
  BRF(K, 21, NO_OF_WAVS) + BRF(K, 31, NO_OF_WAVS) + $
  BRF(K, 32, NO_OF_WAVS) + BRF(K, 42, NO_OF_WAVS) + $
  BRF(K, 43, NO_OF_WAVS) + BRF(K, 53, NO_OF_WAVS) + $
  BRF(K, 54, NO_OF_WAVS) + BRF(K, 64, NO_OF_WAVS) + $

```

```

                BRF(K, 65, NO_OF_WAVS) + BRF(K, 75, NO_OF_WAVS))/12.00
; 60 degs.
R_avg(4) = (BRF(K, 11, NO_OF_WAVS) + BRF(K, 19, NO_OF_WAVS) + $
           BRF(K, 22, NO_OF_WAVS) + BRF(K, 30, NO_OF_WAVS) + $
           BRF(K, 33, NO_OF_WAVS) + BRF(K, 41, NO_OF_WAVS) + $
           BRF(K, 44, NO_OF_WAVS) + BRF(K, 52, NO_OF_WAVS) + $
           BRF(K, 55, NO_OF_WAVS) + BRF(K, 63, NO_OF_WAVS) + $
           BRF(K, 66, NO_OF_WAVS) + BRF(K, 74, NO_OF_WAVS))/12.00
; 45 degs.
R_avg(3) = (BRF(K, 12, NO_OF_WAVS) + BRF(K, 18, NO_OF_WAVS) + $
           BRF(K, 23, NO_OF_WAVS) + BRF(K, 29, NO_OF_WAVS) + $
           BRF(K, 34, NO_OF_WAVS) + BRF(K, 40, NO_OF_WAVS) + $
           BRF(K, 45, NO_OF_WAVS) + BRF(K, 51, NO_OF_WAVS) + $
           BRF(K, 56, NO_OF_WAVS) + BRF(K, 62, NO_OF_WAVS) + $
           BRF(K, 67, NO_OF_WAVS) + BRF(K, 73, NO_OF_WAVS))/12.00
; 30 degs.
R_avg(2) = (BRF(K, 13, NO_OF_WAVS) + BRF(K, 17, NO_OF_WAVS) + $
           BRF(K, 24, NO_OF_WAVS) + BRF(K, 28, NO_OF_WAVS) + $
           BRF(K, 35, NO_OF_WAVS) + BRF(K, 39, NO_OF_WAVS) + $
           BRF(K, 46, NO_OF_WAVS) + BRF(K, 50, NO_OF_WAVS) + $
           BRF(K, 57, NO_OF_WAVS) + BRF(K, 61, NO_OF_WAVS) + $
           BRF(K, 68, NO_OF_WAVS) + BRF(K, 72, NO_OF_WAVS))/12.00
; 15 degs.
R_avg(1) = (BRF(K, 14, NO_OF_WAVS) + BRF(K, 16, NO_OF_WAVS) + $
           BRF(K, 25, NO_OF_WAVS) + BRF(K, 27, NO_OF_WAVS) + $
           BRF(K, 36, NO_OF_WAVS) + BRF(K, 38, NO_OF_WAVS) + $
           BRF(K, 47, NO_OF_WAVS) + BRF(K, 49, NO_OF_WAVS) + $
           BRF(K, 58, NO_OF_WAVS) + BRF(K, 60, NO_OF_WAVS) + $
           BRF(K, 69, NO_OF_WAVS) + BRF(K, 71, NO_OF_WAVS))/12.00
; nadir
R_avg(0) = (BRF(K, 15, NO_OF_WAVS) + BRF(K, 26, NO_OF_WAVS) + $
           BRF(K, 37, NO_OF_WAVS) + BRF(K, 48, NO_OF_WAVS) + $
           BRF(K, 59, NO_OF_WAVS) + BRF(K, 70, NO_OF_WAVS))/6.00
; apply numerical integration technique
RHO(K, NO_OF_WAVS) = TOTAL(R_avg*DeltaOhm(1:6))/!PI
ENDFOR      ; NO_OF_WAVS loop
;*****;
; Index of 400 nm is 64, index of 1195 nm is 472 ;
; calculate ANIX vals. in all azimuth planes ;
;*****;
; neglect the reads. at -10, -8, ..... 8, 10 (noisy)
FOR I = 0, 643 DO BEGIN
; 0 deg.
ANIX[K, 0, I] = MAX(BRF(K, 10:20, I))/MIN(BRF(K, 10:20, I))
; 30 deg.
ANIX[K, 1, I] = MAX(BRF(K, 21:31, I))/MIN(BRF(K, 21:31, I))
; 60 deg.

```

```

ANIX[K, 2, I] = MAX(BRF(K, 32:42, I))/MIN(BRF(K, 32:42, I))
; 90 deg.
ANIX[K, 3, I] = MAX(BRF(K, 43:53, I))/MIN(BRF(K, 43:53, I))
; 120 deg.
ANIX[K, 4, I] = MAX(BRF(K, 54:64, I))/MIN(BRF(K, 54:64, I))
; 150 deg.
ANIX[K, 5, I] = MAX(BRF(K, 65:75, I))/MIN(BRF(K, 65:75, I))

ENDFOR

;*****;
;
;       write ANIX vals. in all planes to a file
;
;*****;
OPENW, Unit, OUTBASEDIR+OUT_DIR[K]+SITES[K]+'ALLANIX.dat', /GET_LUN
PRINTF, Unit, $
'VARIABLES="WAVELENGTH (NM)", "`f_v = 0~0", "`f_v = 30~0", "`f_v =
60~0", "`f_v = 90~0", "`f_v = 120~0", "`f_v = 150~0"'
FOR J = 0, 643 DO BEGIN
  PRINTF, Unit, $
  FLOOR(wavelength(J)), $
  ANIX(K, 0, J), ANIX(K, 1, J), ANIX(K, 2, J), $
  ANIX(K, 3, J), ANIX(K, 4, J), ANIX(K, 5, J)
ENDFOR
FREE_LUN, Unit

;*****;
; Write out mean anix value by summing up ANIX vals. at
; all wavelengths in each azimuth plane
;*****;
OPENW, Unit, OUTBASEDIR+OUT_DIR[K]+SITES[K]+'stats.dat', /GET_LUN
FOR I = 0, 5 DO BEGIN
  ANIX_MEAN[I] = total(ANIX(K, I, 64:556))/493
  PRINTF, Unit, 'Mean ANIX value in plane ', I, ' = ', ANIX_MEAN[I]
ENDFOR
FREE_LUN, Unit

ZENITH = [-75, -60, -45, -30, -15, 0, 15, 30, 45, 60, 75]

;*****;
;
; write BRF vals. in SPP for specific zenith angles
;
;*****;
OPENW, Unit, OUTBASEDIR+OUT_DIR[K]+SITES[K]+'BRFSPP.dat', /GET_LUN

PRINTF, Unit, $
'VARIABLES="WAVELENGTH (NM)", "-75~0", "-60~0", "-45~0", "-30~0", "-
15~0", "0~0", "15~0", "30~0", "45~0", "60~0", "75~0"'
FOR J = 0, 643 DO BEGIN
  PRINTF, Unit, $
  FLOOR(wavelength(J)), $
  BRF(K, 10, J), BRF(K, 11, J), BRF(K, 12, J), $
  BRF(K, 13, J), BRF(K, 14, J), BRF(K, 15, J), $

```

```

        BRf(K, 16, J), BRf(K, 17, J), BRf(K, 18, J), $
        BRf(K, 19, J), BRf(K, 20, J)
    ENDFOR

FREE_LUN, Unit

;*****;
;
; write ANIF vals. in SPP for all zenith angles
;
;*****;
OPENW, Unit, OUTBASEDIR+OUT_DIR[K]+SITES[K]+'ANIFSPP.dat', /GET_LUN

PRINTF, Unit, $
'VARIABLES="WAVELENGTH (NM)", "-75~0", "-60~0", "-45~0", "-30~0", "-
15~0", "0~0", "15~0", "30~0", "45~0", "60~0", "75~0"'

    FOR J = 0, 643 DO BEGIN
        PRINTF, Unit, $
        FLOOR(wavelength(J)), $
        ANIF(K, 10, J), ANIF(K, 11, J), ANIF(K, 12, J), $
        ANIF(K, 13, J), ANIF(K, 14, J), ANIF(K, 15, J), $
        ANIF(K, 16, J), ANIF(K, 17, J), ANIF(K, 18, J), $
        ANIF(K, 19, J), ANIF(K, 20, J)
    ENDFOR

FREE_LUN, Unit

;*****;
; Write BRf vals. in SPP at all wavelengths
; (to plot 3D surface in SPP)
;
;*****;
OPENW, Unit, OUTBASEDIR+OUT_DIR[K]+SITES[K]+'BRFSURFACE.dat', /GET_LUN
PRINTF, Unit, $
'VARIABLES = "ZENITH ANGLE (DEGREES)", "WAVELENGTH (NM)", "BRF"'
PRINTF, Unit, 'ZONE I = 11, J = 409, K = 1, F = POINT'
FOR I = 0, 408 DO BEGIN
    FOR J = 0, 10 DO BEGIN
        PRINTF, Unit, $
        ZENITH(J), $
        FLOOR(wavelength(I+64)), $
        BRf(K, J+10, I+64)
    ENDFOR
ENDFOR

FREE_LUN, Unit

;*****;
; Write ANIF vals. in SPP at all wavelens.
; (to plot 3D surface in SPP)
;
;*****;
OPENW, Unit, OUTBASEDIR+OUT_DIR[K]+SITES[K]+'ANIFSURFACE.dat', /GET_LUN

```

```

PRINTF, Unit, $
'VARIABLES = "ZENITH ANGLE (DEGREES)", "WAVELENGTH (NM)", "ANIF"'
PRINTF, Unit, 'ZONE I = 11, J = 409, K = 1, F = POINT'
FOR I = 0, 408 DO BEGIN
  FOR J = 0, 10 DO BEGIN
    PRINTF, Unit,          $
    ZENITH(J),             $
    FLOOR(wavelength(I+64)), $
    ANIF(K, J+10, I+64)
  ENDFOR
ENDFOR

FREE_LUN, Unit

; neglect the reads. -10, -8, ..., 8, 10 in the SPP (noisy)
; The zenith angles will be the radius (11 pts.)
radius = [-75, -60, -45, -30, -15, 0.000, 15, 30, 45, 60, 75 ]

; The azimuth angles will be the angles for rotation (6 pts.)
angle = [ 0, 30, 60, 90, 120, 150]
angle = angle*(!PI)/180 ; convert to radians

; zed(zen. angle, azi. angle)
; BRF(zen. angle, wavelen. index)
zed = FLTARR(11, 6)

zed(0:10, 0) = BRF(K, 10:20, INDEX)
zed(0:10, 1) = BRF(K, 21:31, INDEX)
zed(0:10, 2) = BRF(K, 32:42, INDEX)
zed(0:10, 3) = BRF(K, 43:53, INDEX)
zed(0:10, 4) = BRF(K, 54:64, INDEX)
zed(0:10, 5) = BRF(K, 65:75, INDEX)

;*****;
;          PARAMETERS          ;
;          FOR GRIDDING & INTERPOLATION          ;
;*****;
ZONEVAL = 151 ; for 1 deg. interp.
INC = 1 ; "
X0 = -90
Y0 = -90
X1 = 90
Y1 = 90

data = POLAR_SURFACE(zed, radius, angle, /GRID, SPACING = [1, 1])

;*****;
;          ;
; Write BRF vals. at all zenith & all azi. (POLAR 3D SURFACE) ;
;          ;
;*****;
OPENW, Unit, OUTBASEDIR+OUT_DIR[K]+SITES[K]+'BRF3D.dat', /GET_LUN
PRINTF, Unit, $
'VARIABLES = "1", "2", "BRF"'

```

```

PRINTF, Unit, $
'ZONE I = '+STRING(ZONEVAL)+' , J = '+STRING(ZONEVAL)+ $
', K = 1, F = POINT'
FOR I = 0, ZONEVAL-1 DO BEGIN
  FOR J = 0, ZONEVAL-1 DO BEGIN
    PRINTF, Unit, $
    INC*I+(-75), INC*J+(-75), data[I, J]
  ENDFOR
ENDFOR

FREE_LUN, Unit

; ANIF(zen. angle, wavelen. index)
zed(0:10, 0) = ANIF(K, 10:20, INDEX)
zed(0:10, 1) = ANIF(K, 21:31, INDEX)
zed(0:10, 2) = ANIF(K, 32:42, INDEX)
zed(0:10, 3) = ANIF(K, 43:53, INDEX)
zed(0:10, 4) = ANIF(K, 54:64, INDEX)
zed(0:10, 5) = ANIF(K, 65:75, INDEX)

data = POLAR_SURFACE(zed, radius, angle, /GRID, SPACING = [1, 1])

;*****;
;
; Write ANIF vals. at all zenith at all azi. (POLAR 3D SURFACE) ;
;
;
;*****;
OPENW, Unit, OUTBASEDIR+OUT_DIR[K]+SITES[K]+'ANIF3D.dat', /GET_LUN
PRINTF, Unit, $
'VARIABLES = "1", "2", "ANIF"'
PRINTF, Unit, $
'ZONE I = '+STRING(ZONEVAL)+' , J = '+STRING(ZONEVAL)+ $
', K = 1, F = POINT'
FOR I = 0, ZONEVAL-1 DO BEGIN
  FOR J = 0, ZONEVAL-1 DO BEGIN
    PRINTF, Unit, $
    INC*I+(-75), INC*J+(-75), data[I, J]
  ENDFOR
ENDFOR

FREE_LUN, Unit

;*****;
; END OF PROCESSING THE DATA SETS ;
;*****;
PRINT, 'Processed data set no.', K
ENDFOR

;*****;
; create o/p data file containing NADIR BRF vals. of all sites ;
; to display only the desired data in tecplot ;
; activate-deactivate the maps accordingly ;
;*****;

```



```

ZENITH_ANGLE = 15

;write o/p to file for tecplot
OPENW, Unit, 'ALL_BRF.dat', /GET_LUN
PRINTF, Unit, $
'VARIABLES="WAVELENGTH (NM)", "valley", "shaded", "peak", "sunny",
"zoysia 1", "zoysia 2", "zoysia 3", "disked", "dry", "hole", "wet",
"flooded"'
  FOR J = 0, 643 DO BEGIN
    PRINTF, Unit, $
    FLOOR(wavelength(J)), $
    BRF(0, ZENITH_ANGLE, J), BRF(1, ZENITH_ANGLE, J), $
    BRF(2, ZENITH_ANGLE, J), BRF(3, ZENITH_ANGLE, J), $
    BRF(4, ZENITH_ANGLE, J), BRF(5, ZENITH_ANGLE, J), $
    BRF(6, ZENITH_ANGLE, J), BRF(7, ZENITH_ANGLE, J), $
    BRF(8, ZENITH_ANGLE, J), BRF(9, ZENITH_ANGLE, J), $
    BRF(10, ZENITH_ANGLE, J), BRF(11, ZENITH_ANGLE, J)
  ENDFOR

FREE_LUN, Unit

;*****;
;
; Create o/p data files containing BRF vals. in the SPP at all ;
; angles for all the test sites. ;
; This is to understand the change in BRF with the viewing ;
; angle with the aid of a movie created in tecplot. ;
; Each file contains the BRFs of all the test sites, thus ;
; there will be 11 such data files ;
;*****;
;write o/p to files for tecplot
ZENITH = [-75, -60, -45, -30, -15, 0, 15, 30, 45, 60, 75]

; start the file names with 1 instead of 0 to adjust for macros in
; tecplot
OUT_FILE = ['1', '2', '3', '4', '5', '6', '7', '8', '9', '10', '11']
FOR ANGLE = 0, 10 DO BEGIN

  OPENW, Unit, OUT_FILE(ANGLE)+'BRF.dat', /GET_LUN
  PRINTF, Unit, $
  'VARIABLES = "WAVELENGTH (NM)"' + ', "valley", "shaded", "peak",
"sunny", "zoysia 1", "zoysia 2", "zoysia 3", "disked", "dry", "hole",
"wet", "flooded"'
    FOR J = 64, 472 DO BEGIN      ; truncate data set

      PRINTF, Unit, $
      FLOOR(wavelength(J)), $
      BRF(0, ANGLE+10, J), BRF(1, ANGLE+10, J), $
      BRF(2, ANGLE+10, J), BRF(3, ANGLE+10, J), $
      BRF(4, ANGLE+10, J), BRF(5, ANGLE+10, J), $
      BRF(6, ANGLE+10, J), BRF(7, ANGLE+10, J), $
      BRF(8, ANGLE+10, J), BRF(9, ANGLE+10, J), $
      BRF(10, ANGLE+10, J), BRF(11, ANGLE+10, J)

    ENDFOR
  ENDFOR

```

```

      FREE_LUN, Unit
ENDFOR

;*****;
;
; Create o/p data files containing ANIX (SPP) vals. of all
; sites, to display only the desired data in tecplot
; activate-deactivate the maps accordingly.
;*****;

;write o/p to file for tecplot
OPENW, Unit, 'ALL_ANIX.dat', /GET_LUN
PRINTF, Unit, $
'VARIABLES="WAVELENGTH (NM)", "valley", "shaded", "peak", "sunny",
"zoysia 1", "zoysia 2", "zoysia 3", "disked", "dry", "hole", "wet",
"flooded"'
  FOR J = 0, 643 DO BEGIN
    PRINTF, Unit, $
      FLOOR(wavelength(J)), $
      ANIX(0, 0, J), ANIX(1, 0, J), $
      ANIX(2, 0, J), ANIX(3, 0, J), $
      ANIX(4, 0, J), ANIX(5, 0, J), $
      ANIX(6, 0, J), ANIX(7, 0, J), $
      ANIX(8, 0, J), ANIX(9, 0, J), $
      ANIX(10, 0, J), ANIX(11, 0, J)
  ENDFOR

FREE_LUN, Unit

;*****;
;
; Create o/p data files containing albedo vals. of all the
; sites. To display only the desired data in tecplot
; activate-deactivate the maps accordingly.
;*****;
;write o/p to file for tecplot
OPENW, Unit, 'ALL_RHO.dat', /GET_LUN
PRINTF, Unit, $
'VARIABLES="WAVELENGTH (NM)", "valley", "shaded", "peak", "sunny",
"zoysia 1", "zoysia 2", "zoysia 3", "disked", "dry", "hole", "wet",
"flooded"'
  FOR J = 0, 643 DO BEGIN
    PRINTF, Unit, $
      FLOOR(wavelength(J)), $
      RHO(0, J), RHO(1, J), RHO(2, J), $
      RHO(3, J), RHO(4, J), RHO(5, J), $
      RHO(6, J), RHO(7, J), RHO(8, J), $
      RHO(9, J), RHO(10, J), RHO(11, J)
  ENDFOR

FREE_LUN, Unit

;*****;
;

```

```

; Investigate the deviation from the true isotropic behaviour ;
; for some sites in order to compare which one is more ;
; isotropic than the other ;
;*****;
; Method:
; Subtract the ANIF at each view angle from 1.00 and add them
; together and then find the average of all 66 view angles.
; Do this for each wavelength and write the avg. value to a file
; K = 3, 7, 8 correspond to HIP4, DISKED AND PACK1
DEV_FROM_ISO = FLTARR(3, 644) ; for three sites and 409 wavelengths

FOR WAV = 0, 643 DO BEGIN

    FOR ANGLE = 0, 65 DO BEGIN
        DEV_FROM_ISO(0, WAV) = $
        DEV_FROM_ISO(0, WAV) + ABS(1.00 - ANIF(3, ANGLE+10, WAV))
        DEV_FROM_ISO(1, WAV) = $
        DEV_FROM_ISO(1, WAV) + ABS(1.00 - ANIF(7, ANGLE+10, WAV))
        DEV_FROM_ISO(2, WAV) = $
        DEV_FROM_ISO(2, WAV) + ABS(1.00 - ANIF(8, ANGLE+10, WAV))
    ENDFOR

    DEV_FROM_ISO(0, WAV) = (DEV_FROM_ISO(0, WAV)/66.0)*100.00
    DEV_FROM_ISO(1, WAV) = (DEV_FROM_ISO(1, WAV)/66.0)*100.00
    DEV_FROM_ISO(2, WAV) = (DEV_FROM_ISO(2, WAV)/66.0)*100.00

ENDFOR

; Write o/p to file for tecplot
OPENW, Unit, 'COMPARE_ANISOTROPY.dat', /GET_LUN
PRINTF, Unit, $
'VARIABLES="WAVELENGTH (NM)", "sunny", "disked", "dry"'
    FOR J = 64, 472 DO BEGIN
        PRINTF, Unit, $
        FLOOR(wavelength(J)), $
        DEV_FROM_ISO(0, J), $
        DEV_FROM_ISO(1, J), $
        DEV_FROM_ISO(2, J)
    ENDFOR

FREE_LUN, Unit

PRINT, 'Total execution time : ', SYSTIME(/SECONDS) - startTime

END

```

```

idl_anif_movie.pro:

;*****;
;
;           ANIMATING DATA SETS           ;
; This program reads in radiances from all the data sets and ;
; calculates the ANIF at all the angles by interpolating them ;
; to 1 degree resolution. ;
; A 3-D plot of the surface ANIFs is created. ;
; This is done for all the wavelengths from 400 to 1200 NM in ;
; order to study the change in BRF and ANIF values with the ;
; wavelength. ;
; The files are used to create a mpeg movie which can be ;
; viewed using mpeg_play program in unix or Media Player in ;
; Windows. ;
; NOTE: Nadir reflectance is used to normalize the ANIF values. ;
;*****;
PRO idl_anif_movie

; for performance measurement
sec = SYSTIME(1)

; path to the directory where the data is located
INBASEDIR = $
'/rstc/user1/erc/pushkar/ruff_goniometer_991203/goniometer/SFG Data/'

IN_DIR = ['North Farm/Hip1/'      , 'North Farm/Hip2/',      $
          'North Farm/Hip3/'      , 'North Farm/Hip4/',      $
          'North Farm/Turf1/'     , 'North Farm/Turf2/',     $
          'North Farm/Turf3/'     ,                          $
          'Ramsey Bottom/Disked/'  ,                          $
          'Ramsey Bottom/Pack1/'   , 'Ramsey Bottom/Pack2/',   $
          'Ramsey Bottom/Pack3/'   , 'Ramsey Bottom/Pack4/']

; path to directory where o/p files will be stored
OUTBASEDIR = '/rstc/user1/erc/pushkar/envipaper1/'
OUT_DIR = 'movies/'

; starting extensions for o/p files
SITES = ['HIP1', 'HIP2', 'HIP3', 'HIP4', $
         'TURF1', 'TURF2', 'TURF3',     $
         'DISKED',                          $
         'PACK1', 'PACK2', 'PACK3', 'PACK4']

name = ' '
BASENAME = STRARR(12)

; these files hold the i/p file name and extensions
file_format_1 = '/rstc/user1/erc/pushkar/envipaper1/GR111199.in'
file_format_2 = '/rstc/user1/erc/pushkar/envipaper1/GR111299.in'

tgtarry = STRARR(76) ; Fixed number of measurements

OPENR,lun, file_format_1, /GET_LUN
READF,lun, name

```

```

READF,lun, tgtarry
tgtarry = STRCOMPRESS(tgtarry)
FREE_LUN, lun

; files in North Farm dir. have this name
BASENAME(0:6) = name

OPENR,lun, file_format_2, /GET_LUN
READF,lun, name
FREE_LUN, lun

; files in Ramsey Bottom dir. have this name
BASENAME(7:11) = name

ext = STRARR(76) ; file name extension

FOR i = 0, 75 DO BEGIN
    tmp = STR_SEP(tgtarry[i], ' ')
    ext[i] = tmp[0]
ENDFOR

SEP = '.'
infile = STRARR(76)

;*****;
; define the variables ;
;*****;

PTS = 644
h = ' '
wavelength = FLTARR(644)
target      = FLTARR(76, 644)
reference   = FLTARR(76, 644)
;SIG Format (wavel., target rad., referen. rad.)
s          = FLTARR(3, PTS)

BRF = FLTARR(12, 76, 644)
ANIF = FLTARR(12, 76, 644)
; wavelength index for which the 3-D polar plot is created
;457 = 1050 nm

RANGE = [2.37, 12.00, 2.81,12.12, 2.4, 2.34, 16.46, 2.69, 1.82, 11.2, $
6.24, 25.0] ; max. ANIF in each site
;*****;
; ;
;          START PROCESSING THE DATA SETS ;
; ;
;*****;
; K is the no. of data sets
FOR K = 0, 11 DO BEGIN

FOR i = 0, 75 DO BEGIN
    infile[i] = INBASEDIR+IN_DIR[K]+BASENAME[K]+SEP+ext[i]
ENDFOR

```

```

;*****;
;
;           read in the data files
;
;*****;

FOR J = 0, 75 DO BEGIN

    ; read in data from one file
    OPENR,lun,infile[J], /GET_LUN

    FOR i = 0, 11 DO BEGIN
        READF, lun, h ; skip header
    ENDFOR

    READF,lun,s

    wavelength      = s(0,*)
    target(J, *)    = s(1,*)
    reference(J, *) = s(2,*)

    FREE_LUN, lun

ENDFOR

;*****;
; change target-reference reading reln.ship
;*****;
FOR J = 10, 20 DO BEGIN
    IF(J NE 16) THEN BEGIN
        reference(J, *) = reference(16, *)
    ENDIF
ENDFOR

FOR J = 21, 31 DO BEGIN
    IF(J NE 27) THEN BEGIN
        reference(J, *) = reference(27, *)
    ENDIF
ENDFOR

FOR J = 32, 42 DO BEGIN
    IF(J NE 38) THEN BEGIN
        reference(J, *) = reference(38, *)
    ENDIF
ENDFOR

FOR J = 43, 53 DO BEGIN
    IF(J NE 49) THEN BEGIN
        reference(J, *) = reference(49, *)
    ENDIF
ENDFOR

FOR J = 54, 64 DO BEGIN
    IF(J NE 60) THEN BEGIN
        reference(J, *) = reference(60, *)
    ENDIF
ENDFOR

```

```

        ENDIF
    ENDFOR

    FOR J = 65, 75 DO BEGIN
        IF(J NE 71) THEN BEGIN
            reference(J, *) = reference(71, *)
        ENDIF
    ENDFOR

;*****;
;
;           replace readings <= 0
;
;*****;
    FOR J = 0, 75 DO BEGIN

        FOR I = 0, 643 DO BEGIN

            IF((target(J, I) LE 0.0) OR (reference(J, I) LE 0.0)) THEN
            BEGIN
                target(J, I) = target(J, (I-1))
                reference(J, I) = reference(J, (I-1))
            ENDIF

        ENDFOR

    ENDFOR

    ENDFOR

; convert wavelengths to string after rounding to display
str_wav = STRING(FLOOR(wavelength))+ ' NM'

;*****;
;
;           calculate ANIF values
;
;*****;
    BRF(K, *, *) = target/reference ; BRF(K, 15, *) - nadir BRF

    FOR J = 0, 75 DO BEGIN
        ANIF(K, J, *) = BRF(K, J, *)/BRF(K, 15, *)
    ENDFOR

; neglect the reads. -10, -8, ..., 8, 10 in the SPP (noisy)
; The zenith angles will be the radius (11 pts.)
radius = [-75, -60, -45, -30, -15, 0.000, 15, 30, 45, 60, 75 ]

; The azimuth angles will be the angles for rotation (6 pts.)
angle = [ 0, 30, 60, 90, 120, 150]
angle = angle*(!PI)/180 ; convert to radians

;*****;
;
;           PARAMETERS
;
;           FOR GRIDDING & INTERPOLATION
;*****;

```

```

zed = FLTARR(11, 6)      ; zed(zen. angle, azi. angle)

!P.FONT = 0             ; H/W fonts
!P.COLOR = 0
!P.BACKGROUND = 255
;DEVICE, SET_FONT = 'Courier*12'

DIM = [650, 500]       ; window dimensions

; IDL provides the backing store (RETAIN=2), ensures
; that the window contents will be read properly
WINDOW, 0, XSIZE = DIM[0], YSIZE = DIM[1], RETAIN=2
WSHOW, 0, ICONIC=0     ; show the window
!ORDER = 1             ; make TVRD() read the image TOP->BOTTOM

mpegID = MPEG_OPEN(DIM)

;*****;
;
; Write ANIF vals. at all zenith & all azi. (POLAR 3D SURFACE) ;
;
;*****;
FOR INDEX = 64, 472 DO BEGIN                               ; 64:472

    ; ANIF(zen. angle, wavelen. index)
    zed(0:10, 0) = ANIF(K, 10:20, INDEX)
    zed(0:10, 1) = ANIF(K, 21:31, INDEX)
    zed(0:10, 2) = ANIF(K, 32:42, INDEX)
    zed(0:10, 3) = ANIF(K, 43:53, INDEX)
    zed(0:10, 4) = ANIF(K, 54:64, INDEX)
    zed(0:10, 5) = ANIF(K, 65:75, INDEX)

    SURFACE, POLAR_SURFACE(zed, radius, angle, /GRID), $
    ZRANGE = [0, RANGE(K)], $
    XSTYLE = 1, $
    YSTYLE = 1, $
    ZSTYLE = 1, $
    XTICKNAME = [-75, -60, -45, -30, -15, 0, 15, 30, 45, 60, 75], $
    YTICKNAME = [-75, -60, -45, -30, -15, 0, 15, 30, 45, 60, 75], $
    XTICKS = 10, $
    YTICKS = 10, $
    XMINOR = 1, $
    YMINOR = 1, $
    ZTICKLEN = 0.01, $
    TITLE = 'Anisotropy Factor', $
    AZ = 15

    XYOUTS, 515, 465, str_wav(INDEX), /DEVICE
    XYOUTS, 60, 90, 'SPP', /DEVICE
    XYOUTS, 430, 15, 'OPP', /DEVICE

    R = TVRD()
    MPEG_PUT, mpegID, /COLOR, FRAME=(INDEX-64), IMAGE=R

ENDFOR

```



```
; delete window after writing each movie
WDELETE, 0

MPEG_SAVE, mpegID, $
FILENAME = OUTBASEDIR+OUT_DIR+SITES[K]+'movie'+'ANIF3D.mpg'
MPEG_CLOSE, mpegID

;*****;
; END OF PROCESSING THE DATA SETS ;
;*****;
PRINT, 'Processed data set no.', K
ENDFOR

PRINT, 'Total execution time was: ', SYSTIME(1) - sec

; end of program
END
```

idl_brf_movie.pro:

```

;*****;
;          ANIMATING DATA SETS          ;
; This program reads in radiances from all the data sets and ;
; calculates the BRF at all the angles by interpolating ;
; them to 1 degree resolution. ;
; A 3-D plot of the surface BRF/ANIFs is created. ;
; This is done for all the wavelengths from 400 to 1200 NM in ;
; order to study the change in BRF and ANIF values with the ;
; wavelength. ;
; The files are used to create a mpeg movie which can be viewed ;
; using mpeg_play program in unix or Media Player in Windows. ;
;*****;
PRO idl_brf_movie

sec = SYSTIME(1) ; for performance measurement

; path to the directory where the data is located
INBASEDIR = $
'/rstc/user1/erc/pushkar/ruff_goniometer_991203/goniometer/SFG Data/'

IN_DIR = ['North Farm/Hip1/'      , 'North Farm/Hip2/',      $
          'North Farm/Hip3/'      , 'North Farm/Hip4/',      $
          'North Farm/Turf1/'      , 'North Farm/Turf2/',      $
          'North Farm/Turf3/'      , ,                          $
          'Ramsey Bottom/Disked/'   , ,                          $
          'Ramsey Bottom/Pack1/'    , 'Ramsey Bottom/Pack2/',      $
          'Ramsey Bottom/Pack3/'    , 'Ramsey Bottom/Pack4/']

; path to directory where o/p files will be stored
OUTBASEDIR = '/rstc/user1/erc/pushkar/envipaper1/'
OUT_DIR    = 'movies/'

; starting extensions for o/p files
SITES = ['HIP1', 'HIP2', 'HIP3', 'HIP4', $
         'TURF1', 'TURF2', 'TURF3',      $
         'DISKED', ,                      $
         'PACK1', 'PACK2', 'PACK3', 'PACK4']

name = ''
BASENAME = STRARR(12)

; these files hold the i/p file name and extensions
file_format_1 = '/rstc/user1/erc/pushkar/envipaper1/GR111199.in'
file_format_2 = '/rstc/user1/erc/pushkar/envipaper1/GR111299.in'

tgtarry = STRARR(76) ; Fixed number of measurements

OPENR,lun, file_format_1, /GET_LUN
READF,lun, name
READF,lun, tgtarry
tgtarry = STRCOMPRESS(tgtarry)
FREE_LUN, lun

```

```

; files in North Farm dir. have this name
BASENAME(0:6) = name

OPENR,lun, file_format_2, /GET_LUN
READF,lun, name
FREE_LUN, lun

; files in Ramsey Bottom dir. have this name
BASENAME(7:11) = name

ext = STRARR(76) ; file name extension

FOR i = 0, 75 DO BEGIN
    tmp = STR_SEP(tgtarry[i], ' ')
    ext[i] = tmp[0]
ENDFOR

SEP = '.'
infile = STRARR(76)

;*****;
; define the variables ;
;*****;

PTS = 644
h = ' '
wavelength = FLTARR(644)
target      = FLTARR(76, 644)
reference   = FLTARR(76, 644)
;SIG Format (wavel., target rad., referen. rad.)
s          = FLTARR(3, PTS)

BRF = FLTARR(12, 76, 644)
; wavelength index for which the 3-D polar plot is created
;457 = 1050 nm

RANGE = [0.65, 0.62, 0.61, 4.15, 1.06, 0.91, 10.0, 0.60, $
0.74, 1.33, 0.78, 0.40] ; max. BRF in each site
;*****;
;
;          START PROCESSING THE DATA SETS ;
;
;*****;
; K is the no. of data sets
FOR K = 0, 11 DO BEGIN

FOR i = 0, 75 do begin
    infile[i] = INBASEDIR+IN_DIR[K]+BASENAME[K]+SEP+ext[i]
ENDFOR

;*****;
;
;          read in the data files ;
;

```

```

;*****;
FOR J = 0, 75 DO BEGIN

    ; read in data from one file
    OPENR,lun,infile[J], /GET_LUN

    FOR i = 0, 11 do begin readf, lun, h ; skip header
    ENDFOR

    READF, lun, s

    wavelength      = s(0,*)
    target(J, *)    = s(1,*)
    reference(J, *) = s(2,*)

    FREE_LUN, lun

ENDFOR

;*****;
; change target-reference reading reln.ship ;
;*****;
FOR J = 10, 20 DO BEGIN
    IF(J NE 16) THEN BEGIN
        reference(J, *) = reference(16, *)
    ENDIF
ENDFOR

FOR J = 21, 31 DO BEGIN
    IF(J NE 27) THEN BEGIN
        reference(J, *) = reference(27, *)
    ENDIF
ENDFOR

FOR J = 32, 42 DO BEGIN
    IF(J NE 38) THEN BEGIN
        reference(J, *) = reference(38, *)
    ENDIF
ENDFOR

FOR J = 43, 53 DO BEGIN
    IF(J NE 49) THEN BEGIN
        reference(J, *) = reference(49, *)
    ENDIF
ENDFOR

FOR J = 54, 64 DO BEGIN
    IF(J NE 60) THEN BEGIN
        reference(J, *) = reference(60, *)
    ENDIF
ENDFOR

FOR J = 65, 75 DO BEGIN
    IF(J NE 71) THEN BEGIN

```

```

        reference(J, *) = reference(71, *)
    ENDIF
ENDFOR

;*****;
;
;           replace readings <= 0
;
;*****;
FOR J = 0, 75 DO BEGIN
    FOR I = 0, 643 DO BEGIN
        IF((target(J, I) LE 0.0) OR (reference(J, I) LE 0.0)) THEN
        BEGIN
            target(J, I) = target(J, (I-1))
            reference(J, I) = reference(J, (I-1))
        ENDIF
    ENDFOR
ENDFOR

; convert wavelengths to string after rounding to display
str_wav = STRING(FLOOR(wavelength))+ ' NM'

;*****;
;
;           CALCULATE BRV VALUES
;
;*****;
BRV(K, *, *) = target/reference ; BRV(K, 15, *) - nadir BRV

; neglect the reads. -10, -8, ....., 8, 10 in the SPP (noisy)
; The zenith angles will be the radius (11 pts.)
radius = [-75, -60, -45, -30, -15, 0.000, 15, 30, 45, 60, 75 ]

; The azimuth angles will be the angles for rotation (6 pts.)
angle = [ 0, 30, 60, 90, 120, 150]
angle = angle*(!PI)/180 ; convert to radians

;*****;
;           PARAMETERS
;           FOR GRIDDING & INTERPOLATION
;*****;
zed = FLTARR(11, 6) ; zed(zen. angle, azi. angle)

!P.FONT = 0 ; H/W fonts
!P.COLOR = 0
!P.BACKGROUND = 255
;DEVICE, SET_FONT = 'Courier*12'

DIM = [650, 500] ; window dimensions

; IDL provides the backing store (RETAIN=2), ensures
; that the window contents will be read properly
WINDOW, 0, XSIZE = DIM[0], YSIZE = DIM[1], RETAIN=2
WSHOW, 0, ICONIC=0 ; show the window
!ORDER = 1 ; TVRD() must read the image TOP->BOTOM

```

```

mpegID = MPEG_OPEN(DIM)

;*****;
;
; Write BRF vals. at all zenith & all azi. (POLAR 3D SURFACE) ;
;
;*****;
FOR INDEX = 64, 472 DO BEGIN ; 64:472

    ; BRF(zen. angle, wavelen. index)
    zed(0:10, 0) = BRF(K, 10:20, INDEX)
    zed(0:10, 1) = BRF(K, 21:31, INDEX)
    zed(0:10, 2) = BRF(K, 32:42, INDEX)
    zed(0:10, 3) = BRF(K, 43:53, INDEX)
    zed(0:10, 4) = BRF(K, 54:64, INDEX)
    zed(0:10, 5) = BRF(K, 65:75, INDEX)

    SURFACE, POLAR_SURFACE(zed, radius, angle, /GRID), $
    ZRANGE = [0, RANGE(K)], $
    XSTYLE = 1, $
    YSTYLE = 1, $
    ZSTYLE = 1, $
    XTICKNAME = [-75, -60, -45, -30, -15, 0, 15, 30, 45, 60, 75], $
    YTICKNAME = [-75, -60, -45, -30, -15, 0, 15, 30, 45, 60, 75], $
    XTICKS = 10, $
    YTICKS = 10, $
    XMINOR = 1, $
    YMINOR = 1, $
    ZTICKLEN = 0.01, $
    TITLE = 'Bidirectional Reflectance Factor', $
    AZ = 15

    XYOUTS, 515, 465, str_wav(INDEX), /DEVICE
    XYOUTS, 60, 90, 'SPP', /DEVICE
    XYOUTS, 430, 15, 'OPP', /DEVICE

    R = TVRD()
    MPEG_PUT, mpegID, /COLOR, FRAME=(INDEX-64), IMAGE=R

ENDFOR

; delete window after writing each movie
WDELETE, 0

MPEG_SAVE, mpegID, $
FILENAME = OUTBASEDIR+OUT_DIR+SITES[K]+'movie'+'BRF3D.mpg'

MPEG_CLOSE, mpegID

;*****;
; END OF PROCESSING THE DATA SETS ;
;*****;
PRINT, 'Processed data set no.', K

```

```
ENDFOR
```

```
PRINT, 'Total execution time was: ', SYSTIME(1) - sec
```

```
; end of program
```

```
END
```